PCCP

Intrinsic Interactions of Metal Ions with Biological Molecules as Studied by Threshold Collision-Induced Dissociation and Infrared Multiple Photon Dissociation

Journal:	*Physical Chemistry Chemical Physics*
Manuscript ID	CP-TRV-02-2024-000897.R1
Article Type:	Perspective
Date Submitted by the Author:	09-Jul-2024
Complete List of Authors:	Armentrout, Peter; University of Utah, Chemistry

Submitted to *Phys. Chem. Chem. Phys.*

Perspective: Intrinsic Interactions of Metal Ions with Biological Molecules as Studied by Threshold Collision-Induced Dissociation and Infrared Multiple Photon Dissociation

P. B. Armentrout

Department of Chemistry, University of Utah, Salt Lake City, UT 84112

Abstract. In this perspective, gas-phase studies of group 1 monocations and group 12 dications with amino acids and small peptides are highlighted. Although the focus is on two experimental techniques, threshold collision-induced dissociation and infrared multiple photon dissociation action spectroscopy, these methods as well as complementary approaches are summarized. The synergistic interplay with theory, made particularly powerful by the small sizes of the systems explored and the absence of solvent and support, is also elucidated. Importantly, these gas-phase methods permit quantitative insight into the structures and thermodynamics of metal cations interacting with biological molecules. Periodic trends in how these interactions vary as the metal cations get heavier are discussed as are quantitative trends with changes in the amino acid side chain and effects of hydration. Such trends allow these results to transcend the limitations associated with the biomimetic model systems.

Introduction

In biological systems, metals are generally charged because they interact strongly with coordination sites and solvent. These interactions are primarily noncovalent and electrostatic, and as a consequence, are largely non-directional. This means that the ion can interact with many components of its surroundings (including solvent) simultaneously, making it difficult to quantitatively characterize the strengths of individual components of such interactions.

Some level of quantitative information can be achieved by investigating metal interactions with biological molecules in the gas phase. By eliminating solvent and substrate effects, pairwise interactions in biological systems can be measured with accuracy and precision, both for simple and for more complex interactions that evolve with larger systems. In many cases, the use of model biomimetic systems can simplify and focus the pairwise interactions being studied. In the past, we have described such an approach as developing a thermodynamic "vocabulary" for metal ion interactions in biological systems.[1] Similar to literature, if one has a suitable vocabulary, it should be possible to generate the "*phrases, sentences, paragraphs, and book chapters*" that comprise real biological systems.

It can also be realized that gas-phase studies allow a direct comparison with high-level theoretical results. These comparisons play several important roles. Theory can provide molecular information (vibrational and rotational constants and electronic states) that enhances the interpretation of experimental data. Comparisons between experiment and theory often provide more detailed structural information than is available just from the experimental results. Computations can elucidate subtle features in how metal cation affinities vary with the metal and the properties of the biological molecules. Such trends (elucidated below) transcend the gas-phase and allow application to condensed phase systems. In contraposition, experimental data can provide important benchmarks regarding which levels of theory are adequate approaches (and how accurate) for describing metal interactions with biological molecules.

In this perspective, the focus is on studies of metal cations interacting with amino acids and small peptides. Not included are similar studies of nucleobases, nucleosides, and nucleotides for which there is also a considerable quantitative database.[2-17] Two experimental techniques utilized by the author are highlighted, but other useful approaches and their results are also provided.

Experimental and Theoretical Methods

Because metallated biological systems are generally charged, such complexes can be readily studied using several mass spectrometric (MS) techniques in the gas phase. These

techniques have the advantage of being able to identify the complexes being studied according to their mass-to-charge ratio (*m/z*). In order to obtain more specific thermodynamic and structural information, simple MS approaches must be combined with more advanced methods. Here, several gas-phase experimental and theoretical approaches are introduced that are capable of quantitatively exploring metal ion interactions with biomolecules. Details of these methods can be found in the literature references provided with this brief overview of the methods.

Threshold Collision-Induced Dissociation Experiments

Tandem mass spectrometry (MS/MS) experiments provide a means of investigating the structure of ionized molecules. Such experiments utilize the ability to accelerate charged molecules to high velocities using electric fields. At such high energies, if the accelerated ions collide with neutral molecules, they can undergo additional processes, either reactions or simple translational to internal energy transfer, in which case fragmentation of the ion can ensue. If the neutral molecule is unreactive (e.g., one of the rare gases), the experiments are generally known as collision-induced dissociation (CID), or alternatively collisional activation (CA) or collision-activated dissociation (CAD), where a distinction regarding single versus multiple collisions is made by some investigators. In CID experiments, the dissociation processes observed depend on how much energy is transferred to the ion along with the complexity of the ion. A more subtle effect involves the time scale available in the experiment for fragmentation to occur because large molecules can take longer to dissociate than the experimental time available (generally ms to μs).

Analytical applications of CID include sequencing of biomolecules such as peptides, proteins, and nucleic acids.[18] As peptide (or phosphate ester) bonds are cleaved along the biomolecular backbone, a sequence of fragment ions is produced and can be identified by measuring the masses of the fragment ions. If the fragmentation is complete enough, the results can be analyzed to yield the sequence of amino acids (or nucleobases) of the original biomolecule.

More rare are experiments that utilize CID to quantitatively measure fragmentation thermodynamics. Such experiments are called threshold CID experiments (TCID) or energy-

resolved MS (ERMS).[19] Such measurements are more demanding because a number of effects need to be considered in performing the experiments and analyzing the data. In the best experiments, ions that have characterized internal energies are subjected to single collisions with an inert gas and the collision energy is varied from zero to energies well above those needed for fragmentation (by at least a factor of four). The kinetic-energy dependent processes can be analyzed to extract the energy at which fragmentation begins, the threshold energy.[20-23] This energy is a direct measure of the energy difference between the reactant ion and the rate-limiting transition state leading to the fragmentation. The most quantitative studies of this kind have been performed using a guided ion beam tandem mass spectrometer (GIBMS),[24] although commercially available instruments (e.g., triple quadrupole MS, QQQ) can be used to provide qualitatively similar information. A GIBMS is specifically designed for such TCID experiments because it includes ion sources that provide thermalized ion reactants, it permits well-controlled collision energies over a broad range, and it collects, transmits, and detects reactant and product ions very efficiently.[24]

An example is shown in Figure 1 for the Cs^+(Ser) complex colliding with Xe and dissociating exclusively to form Cs^+ + Ser .[25] Here, the ions were formed by electrospray ionization (ESI), passed into vacuum through a capillary, collected by a radio-frequency (rf) ion funnel, and then passed through an rf hexapole ion guide[26] where the ions are thermalized by >10,000 collisions with ambient gases (largely the ESI solvent).[26-30] Note that the fragmentation probability is reported as a cross section, which describes the absolute probability that the reactants collide and lead to dissociation. When cross sections are multiplied by the relative reactant velocity, one obtains microcanonical rate constants for reaction as a function of the collision energy. Also the energy scale is reported both as the laboratory energy (upper scale), which is the voltage difference between the source and collision region, E_{lab} (and the zero of energy is measured carefully using retarding methods in the octopole),[24] and the center-of-mass (CM) scale, E_{CM}, which describes the energy available to induce reaction (dissociation in this case). This conversion, $E_{CM} = E_{lab} \times m_{Xe} / (m_{Xe} + m_{ion})$ where m_x is the mass of x, is needed because linear momentum conservation demands that

the energy of the entire reaction system moving through the laboratory must be conserved and therefore is unavailable for reaction.

Accurate thermodynamic information from TCID experiments requires data analysis that considers translational energy distributions,[24] the internal energy ion distributions,[31] effects of multiple ion-molecule collisions,[32] lifetimes for ion dissociation,[33] competition between fragmentation channels,[34, 35] tight versus loose transition states,[36, 37] and effects of sequential dissociations.[38] The analysis techniques used to model these effects are detailed in the literature[39] and illustrated in Figure 1. Here, the full line reproducing the data (which has been corrected to single collisions by examining the pressure dependence of the cross section) includes all the effects just noted, whereas the dashed line has removed the energy distributions. Where the dashed line deviates from zero cross section is the threshold energy, here 1.06 ± 0.04 eV = 102 ± 4 kJ/mol,[25] which equals the 0 K bond energy for Cs^+-Ser because there is no reverse barrier to the dissociation, i.e., a loose transition state. This value also includes a correction for lifetime effects of 0.04 eV.[33]

TCID methods have proven to provide accurate thermodynamic information. Although TCID methods have been applied to many systems for which there are no experimental thermochemical data for benchmarking, a number of systems where equilibrium experiments (see below) are available yield good agreement (within about 5 kJ/mol, on the order of the experimental uncertainty in either method).[40-46] In other cases, comparisons with theoretically calculated thermochemistry demonstrate that the TCID results are generally accurate within ~10 kJ/mol.[28, 47-53] For instance, in the Cs^+(Ser) case, four different levels of theory indicate a bond energy ranging from 98 to 112 kJ/mol.[25]

It can also be recognized that the determination of thermodynamic information is a valuable means of determining the structure of the fragment ions produced.[28, 48, 49, 54-56] This requires a comparison with theoretical thermochemistry and is generally restricted to systems where the energetic difference between isomers or conformers is on the order of 5 kJ/mol or more.

Infrared Multiple Photon Dissociation Experiments

A more sensitive and versatile way of obtaining structural information on gas-phase ions is by measurement of their infrared (IR) spectrum, which again necessitates a comparison with theory. This generally involves studies in either the fingerprint region, 500 – 2000 cm^{-1}, or the hydrogen stretching region, 2800 – 3600 cm^{-1}. Because the concentrations of ions are not easily raised to levels needed for absorption measurements, these experiments require so-called "action" spectroscopies in which absorption of a photon (or multiple photons) induces fragmentation that is easily monitored using MS. There are two main variants: "tagging" IR photodissociation (IRPD)[57] and IR multiple photon dissociation (IRMPD).[58, 59] In the former, a weakly bound species (a rare gas atom, H_2, or N_2) attached to the ion of interest is readily lost upon absorption of a single IR photon. Such tagged molecules can only be generated using cryogenic conditions and the tagging species can conceivably perturb the absorption spectrum. In the IRMPD experiment, the ion of interest is interrogated directly by the absorption of many IR photons. Now, generation of the ions is routine but the IR laser needs to have much higher power in order to provide sufficient fluence for the absorption of multiple photons. Such power is often provided by free electron lasers (FELs) but optical parametric oscillators (OPOs) can also be used. Here too, the spectrum can be distorted because of the need to absorb multiple photons (often to the red to compensate for the anharmonicity of vibrational modes). It can also be realized that IRMPD relies on efficient intramolecular vibrational redistribution (IVR),[60, 61] where the energy provided by absorption of a photon into a specific vibrational mode is rapidly moved into other vibrational modes. This process permits the absorption of additional photons at the same photon frequency.[62, 63] IVR requires high rovibrational state densities that are easily provided by metallated biomolecules.

Structural information is provided by IRMPD results through the comparison of the experimental IRMPD spectrum with that generated from quantum chemical calculations (see below). Because the former is a multiple photon process and the latter corresponds to absorption of a single photon, differences can occur both in position (shifts associated with the anharmonicity of the vibrational mode, often corrected by using a frequency scaling factor) and intensity (with predicted weak bands showing little or no experimental intensity

because too few photons are absorbed to induce efficient fragmentation). Generally, there are diagnostic bands in IRMPD spectra that can be strongly associated with the spectrum calculated for a single low-energy conformer or isomer of the interrogated ion, allowing accurate identification of the structure of the species.

An example is shown in Figure 2 for Cs^+(Ser), which is a somewhat complicated case because the spectrum cannot be assigned to a single species.[64] Details of the theory and the nomenclature are introduced below, but the assignment of the experimental spectrum (top panel) is performed as follows. The sharp band observed at 1750 cm^{-1} (associated with a carbonyl stretch) can be reproduced by either the [N,CO,OH] (second panel) or [COOH] (third panel) structures, which also reproduce the band near 1600 cm^{-1}. The [N,CO,OH] structure also reproduces bands observed at 960, 1110, and 1150 cm^{-1} as well as minor bands at 590 and 650 cm^{-1}; however, this structure does not yield any intensity needed to reproduce the strong band at 1400 cm^{-1}. This band can be associated with the [COOH] structure, which also contributes intensity in the 800 – 1200 region including the bands at 880 and 1050 cm^{-1}. Left unaccounted for is the band observed at 1670 cm^{-1}, which is consistent with a contribution from the [CO_2^-] (bottom panel) structure that also helps explain the broadening observed for the 1400 cm^{-1} band to the red. We therefore concluded that all three structures must be present under the experimental conditions used.[64]

Theoretical Calculations

As noted above, the experimental studies of metal cations interacting with biological molecules often rely on theory to provide molecular parameters needed to interpret the data, energies of fragmentation processes for comparison with TCID experiments, and IR spectra for comparison to IRMPD results. The synergy between experiment and theory provides more robust and detailed results than could be achieved without the computations.

Of course, there are a wide array of different levels of theory that a suitable for examining cationized biomolecules. In our laboratory, we have settled on a workflow that appears to provide accurate structural and thermodynamic information for most metal-biological molecule systems. Using the Gaussian suite of programs,[65] all-electron calculations are performed for smaller systems, generally using a 6-311+G(d,p) triple-ζ basis set that

includes polarization (d,p) and diffuse (+) functions for the lighter alkali metals (Li, Na, and K). For first-row transition metals, we either use the same Pople basis sets or the def2-TZVP basis set, which is a balanced basis set at the triple-ζ level including polarization (P) functions. For the heavier Rb and Cs alkali and Cd metal systems, we use the def2-TZVP basis sets that incorporate small-core effective core potentials (ECPs) developed by Leininger et al.[66] As the systems get larger, a simulated annealing approach is used to explore the associated conformational space and determine low-energy conformers.[67-71] Each unique conformer is then geometry optimized using B3LYP with a double zeta basis set before the protocol described above is initiated.

These geometry optimizations are accompanied by calculations of the vibrational frequencies and are usually performed using the B3LYP density functional[72, 73] or B3LYP with dispersion corrections (GD3BJ),[74, 75] as we have found that more time-consuming second-order Möller-Plesset (MP2) geometry optimizations[76] yield very similar results. We follow these geometry optimizations with single-point energy calculations performed using larger basis sets, 6-311+G(2d,2p), def2-TZVPP, or def2-TZVPPD (where D indicates diffuse functions), which are required to yield accurate energetics.[50] Such single-point calculations are usually performed at multiple levels of theory, B3LYP, B3LYP-GD3BJ, and MP2(full) (where full indicates correlation of all electrons), along with B3P86 or M06[77] approaches in some cases. In rare cases, we have also applied the coupled cluster with single, double, and perturbative triple excitations, CCSD(T), method[78, 79] to these types of systems;[80] however, this high-quality approach becomes increasingly inaccessible as the systems increase in size. Moving forward, we also intend to apply the range-separated hybrid ωB97M-V functional[81] to these types of systems because its performance relative to CCSD(T) was better than other density functional approaches,[80] as discussed further below. We *always* include multiple computational approaches because different levels of theory often do not agree on the relative energies of low-lying conformations, as illustrated further below. Further, theoretical metal cation-ligand BDEs generally exhibit a spread in values that is often comparable to experimental uncertainties.

Single-point energies are corrected for zero-point energies (ZPE) calculated at the lower levels of theory used for geometry optimizations. This permits calculation of the thermochemistry at 0 K, and thermal corrections (assuming the rigid-rotor and harmonic oscillator approximation) are applied to yield 298 K thermodynamic values. Both ZPE and thermal corrections use scaling factors appropriate for the particular method and basis set used, as outlined elsewhere.[82] Theoretical bond dissociation energies (BDEs) are calculated by the difference in the ZPE-corrected single-point energies of products minus reactants. Reported BDEs also include basis set superposition error (BSSE) corrections at the full counterpoise level.[83, 84]

The lightest alkali cation, Li^+, has been found to exhibit one interesting property that alters the general approach noted above. When ligands are strongly bound to Li^+, there are repulsive interactions with the 1s core electrons of the cation.[85] To account for this effect, the core electrons must be permitted to polarize away from the ligand, which requires using the correlation consistent polarized core/valence basis sets (cc-pCVXZ where X = D, T, and Q) of Dunning for lithium[86] and aug-cc-pVXZ basis sets on all other atoms for consistency. Using the MP2(full) level of theory and a complete basis set extrapolation, this procedure yields thermodynamic values in agreement with experiment. We also recommended that an adequate level of theory is provided by a MP2(full)/aug-cc-pVTZ(Li-C)//MP2(full)/cc-pVDZ(Li-C) approach, where (Li-C) indicates the cc-pCVXZ basis set on Li.[85] All def2 and cc-pCVXZ basis sets can be obtained from the Basis Set Exchange.[87-89]

In cases where theory is used to predict infrared spectra, the predicted harmonic frequencies are generally scaled to account for known inaccuracies in the calculated frequencies. In many cases, we have found that B3LYP/6-311+G(d,p) spectra accurately reproduce experiments using a scaling scaling factor of 0.975, although a recent study notes that this can vary between 0.97 and 0.98.[80] Before comparison with experiment, the calculated frequencies are also broadened to account for the finite laser bandwidth, unresolved rotational envelope, anharmonic broadening of the vibrational bands, and broadening resulting from the multiple-photon absorption process. (For example, the spectra in Figure 2b-d are broadened using a 20 cm^{-1} full width at half maximum Gaussian

distribution.) Strongly anharmonic vibrational modes may not be adequately predicted by harmonic frequency calculations, but such instances are often consistent from system to system (e.g., the NH_2 scissors mode near 1600 cm^{-1} of metalated amino acids is often blue shifted compared to experiment by ~30 cm^{-1}).[64, 90-95] Because the comparisons are between experimental spectra corresponding to multiple photon absorption and IR spectra that relate to single photon absorption, the intensities can vary between the theoretical and experimental spectra. This often results in weaker modes not being observed because insufficient number of photons are absorbed to lead to efficient photodissociation.

As will be found below, theory is also used to calculate isotropic molecular polarizabilities of neutral molecules, which are needed for thermochemical analysis of TCID data as well as the examination of periodic trends. The PBE0/6-311+G(2d,2p) level of theory has been shown to provide polarizabilities that are in good agreement with measured values.[96]

Other Experimental Approaches

In addition to the TCID and IRMPD methods discussed above, thermodynamic information and structural information can also be obtained using other experimental methods. Very reliable thermochemistry can be obtained using techniques that rely on bringing the reactants and products into equilibrium and measuring their concentrations as a function of temperature. A van't Hoff plot can then be used to convert the measured equilibrium constant to the enthalpies and entropies of the reaction. Such studies can be pursued at both low and high pressures in the presence or absence of buffer gases. When successful, this method can provide rigorous thermodynamic determinations but is subject to uncertainties associated with whether the ion sampling perturbs the equilibrium and with the absolute temperature. This method has been used to measure the relative binding energies of metal cations to a wide range of ligands[97, 98] and hydration energies.[99-102] Not that many biological systems have been included mainly because such samples are not always volatile.

A related method is blackbody infrared radiative dissociation (BIRD), in which ions are allowed to equilibrate with their thermal surroundings by absorption of background blackbody infrared radiation.[103, 104] By quantitatively measuring the extent of dissociation as a

function of the temperature, thermodynamic information can be extracted using master equation modeling.[105]

Another more qualitative (but also more easily applied) approach to thermodynamic methods is the kinetic method, introduced by Cooks and coworkers.[106, 107] Here, the relative intensities of products resulting from dissociation of a cation (or anion) bound dimer are measured and presumed to represent a quasi-equilibrium. The methods of analyzing such data have been revised extensively to try and include important entropic effects.[108, 109] The limitations of this approach have been discussed thoroughly.[110-112] Ultimately, the kinetic method is primarily limited by the fact that the temperature of the thermodynamic information is ill-defined; however, this approach can certainly provide useful relative information.

Structural information can also be obtained using ion mobility, in which ions are pulled through a bath gas (often He or N_2) by an electric field.[113-115] Larger ions move more slowly than smaller ions, such that a measurement of the rate at which the ions move a set distance provides the rotationally averaged size of the ion. By comparing this experimental size with computational structures, assignments of the structures of ions can be inferred, although the precision of this technique permits only fairly large changes (e.g., folded versus extended peptides) to be identified.

Alkali Metal Cations Interacting With Glycine

Sodium and Potassium

One means of appreciating how metal ions interact with a multi-functional molecule such as an amino acid is to evaluate each of the functional groups independently. This approach has been pursued for both sodium and potassium cations, specifically with regard to their interactions with the simplest amino acid, glycine (Gly). Here, the molecules that represented the various functional components of Gly were 1-propyl amine (for NH_2), 1-propanol (for OH), methyl ethyl ketone (MEK, for the CO carbonyl) as well as pairs of these, propionic acid (PPA, for the COOH group), and ethanol amine (for NH_2 and OH). For the sodiated complexes,[116] the order of the binding affinity for molecules having a single functional group

was OH < NH_2 < CO, whereas for potassiated complexes,[117] the order was NH_2 < OH < CO. Thus, the primary binding site for both alkali cations is the carbonyl, but the smaller Na^+ cation prefers binding to NH_2 and the larger K^+ cation prefers binding to OH.

The preference for binding to the carbonyl oxygen is even more apparent when the BDEs of MEK are compared to PPA. Na^+ and K^+ bind more strongly to MEK by 13 and 9 kJ/mol compared to PPA, even though theory indicates that the metal cation binds to both oxygens of PPA. This difference occurs because the optimum bonding angle for the metal cation (M) to the carbonyl is near 180°, i.e., directed along the carbonyl dipole. In contrast, the bidentate binding in PPA leads to a much less optimal ∠MOC bond angle, coupled with an inductive effect of the hydroxyl group that reduces electron density on the carbonyl oxygen.

The OH < NH_2 < CO ordering found for sodium is consistent with the IRMPD experimental finding[118, 119] that Na^+ interacts with Gly by bidentate binding to the carbonyl and the amino group, which we designate as [N,CO], Figure 3. Compared with MEK, the bidentate binding to glycine leads to stronger binding with Na^+ by 33 kJ/mol. Interestingly, ethanol amine binds Na^+ more tightly than Gly by 11 kJ/mol, even though the favored carbonyl group has been replaced by the hydroxy ligand site. We believe this occurs because the sp^3 carbons in ethanol amine allow better overlap of the heteroatom lone pairs with the metal cation, whereas sp^2 hybridization at the carboxylic acid group of Gly leads to conformational restrictions.

When a similar analysis is conducted for potassium ion complexes,[117] the relative results are similar although the absolute BDEs are 74 ± 4% of those for Na^+; however, K^+ binds the amino group only 67% as strongly as Na^+. As noted above, this changes the BDE order of molecules with single functional groups, NH_2 < OH < CO. As a consequence, theory indicates that K^+ no longer binds to glycine as [N,CO] coordination. Rather it prefers binding either via the two oxygen atoms in the carboxylic acid group, i.e., a [CO,OH] global minimum structure, or just to the carbonyl oxygen, [CO], Figure 3.[119] Theory places the [N,CO] isomer, like that found for Na^+(Gly), 2 – 9 kJ/mol higher in energy. Notably, the [CO,OH] and [CO] isomers are stabilized by an OH•••N hydrogen bond. Further, this geometry corresponds to the global minimum structure of isolated glycine. Experimentally,

the IRMPD spectrum of K^+(Gly) is reproduced well by the calculated spectrum of either of these two isomers, which are similar. When an anharmonic vibration calculation was performed (with no frequency scaling), the [CO,OH] spectrum matched the experimental spectrum particularly well and we concluded that this was the dominant species present.[119] This agrees with relative energetics calculated at the MP2 and CCSD(T) levels, but not those calculated using DFT approaches (B3LYP and B3LYP-GD3BJ).

An interesting and important aspect of the [CO,OH] and [CO] isomers is that they are linked in a double-well potential corresponding to changing the ∠MOC bond angle. Figure 4a shows this for the example of potassiated alanine (Ala).[80, 120] The [CO,OH] isomer is also linked to the [CO_2^-] isomer by moving the hydroxy proton to the amino group, thereby yielding a zwitterionic structure, Figure 4b, but this generally requires more energy in gas-phase complexes.[80, 120] Different levels of theory make drastically different predictions regarding the relative stability of the coupled wells.[120] This phenomenon has been explored in increasing detail for the Cs^+(Gly) complex, described below.

Lithium and Rubidium

For Li^+, according to both IRMPD experiments and theory, binding to glycine matches that observed for Na^+, i.e., [N,CO], consistent with the higher charge density on these smaller cations.[119] Indeed, alternative isomers are now much higher in energy than those of the larger alkali cations. Like K^+, theory indicates that Rb^+ prefers either the [CO,OH] or [CO] isomers, again linked by a double-well potential. Compared with K^+(Gly), the MP2 potential well for [CO] disappears, whereas the DFT levels still indicate a [CO] global minimumstructure along with stabilization of the [CO,OH] isomer of the Rb^+(Gly) complex. Comparison of the theoretical spectra with the IRMPD spectrum for Rb^+(Gly) indicates that both species are present, with the [CO] spectrum providing a slightly better match to the carbonyl stretch observed at 1726 cm^{-1} (although this conclusion relies on how the frequencies are scaled, as discussed further next).

Cesium

In our original work on the Cs^+(Gly) complex, we made a parallel conclusion that the [CO] isomer explained the observed IRMPD spectrum.[119] We recently revisited this system

(in conjunction with other aliphatic amino acids, see below) and performed additional high-level calculations.[80] In interpreting the data, we also allowed the frequency scaling factor to vary rather than using a fixed scaling factor of 0.975 as used in the previous work. Although the 0.975 factor works well for B3LYP calculations, this level of theory does not yield a stable [CO,OH] isomer for Cs^+(Gly), hence this isomer was calculated at the MP2 level previously.[119] In our reevaluation,[80] we calculated both spectra at the B3LYP-GD3BJ level, as this calculation yielded stable species for both isomers. The scaling factor was then chosen so that the calculated carbonyl stretch matched experiment: 0.98 for [CO] and 0.97 for [CO,OH]. This comparison suggested that the spectrum for the [CO,OH] isomer matched experiment somewhat better, in contrast with our previous conclusion. One notable discrepancy between the calculated and experimental spectra was a calculated band at 950 cm^{-1} (for both isomers) that was not observed. This calculated band corresponds to an out-of-plane OH wag. A spectrum calculated at the CCSD level of theory shifts this band to 902 cm^{-1} where it overlaps a band at 895 cm^{-1} (NH_2 wag), which match an experimental band at 884 cm^{-1}. Here, the experimental spectrum was well reproduced by the CCSD spectrum calculated for the [CO,OH] isomer.

We also performed a more complete examination of the double-well potential calculated at various levels of theory. MP2 and CCSD(T) calculations agree that the [CO] isomer collapses to [CO,OH], whereas B3LYP concludes the opposite. Adding dispersion corrections, B3LYP-GD3BJ, stabilizes the [CO,OH] isomer creating the double-well potential, but [CO] is still the lower energy structure. The range-separated hybrid ωB97M-V functional[81] yields a potential surface that lies in between the CCSD(T) and B3LYP-GD3BJ surfaces, with the [CO,OH] isomer being the global minimum structure, but [CO] still being a stable species, i.e., again a double well potential.

The reason for these disparate results was explored in some detail. One simple factor is the need to include electron correlation in determining the relative energies of the [CO,OH] and [CO] isomers. Another contributor is the tendency of DFT to delocalize charge.[121] In the Cs^+(Gly) complex, this influences the strength of the OH•••N hydrogen bond, with DFT tending to increase its strength.[122] Spectroscopically, this difference is verified by the out-of-

plane OH wag band described above. CCSD places this wag at 902 cm^{-1}, whereas the DFT methods shift this band to higher frequencies, *inconsistent* with experiment. Theory predicts this should also influence the OH stretch, which experiment indicates is severely broadened by the OH•••N hydrogen bond.[80]

Periodic Trends in Binding Energies

When comparing the BDEs of the five alkali cations to any particular ligand, one finds that the values increase as the size of the metal cation decreases.[123-125] This is a simple electrostatic effect in that the smaller cation has a shorter bond distance leading to a stronger bond. Glycine, or for that matter any other amino acid or small peptide, is no exception. This electrostatic effect dominates the trends in the BDEs even though the specific isomer that corresponds to the global minimum structure can change as the size of the alkali cation increases, as described above. Interestingly, the BDEs to Gly increase linearly with the inverse of the ionic radius, as shown in Figure 5, consistent with a largely electrostatic interaction.

Effects of Hydration

We have also examined how a sodium ion interacts with glycine as water molecules are added. TCID measurements allowed the determination of the energies required for both water loss (the dominant CID process) and glycine loss from $Na^+(Gly)(H_2O)_x$ complexes where x = 1 – 4. Bond energies for loss of water and glycine decline monotonically with increasing hydration from 75 ± 5, 55 ± 7, 40 ± 5, and 32 ± 8 kJ/mol for x = 1 to 4, respectively. The experimental BDEs are reproduced reasonably well by several levels of theory. The observed decline is found because as additional ligands are added there is increased ligand-ligand repulsion and the effective charge on the sodium cation decreases.

Theory indicates that addition of one water molecule occurs directly to the sodium ion in the [N,CO] isomer of Na^+(Gly), whereas additional water molecules preferentially stabilize the [CO] isomer. Notably, this includes a water molecule bound to the Na^+ site with a hydrogen bond to the hydroxy oxygen, HOH•••OH•••N. Theory also suggests that the zwitterionic form of this complex (i.e., $[CO_2^-]$, Figure 3) becomes more stable with additional water ligands as well, in particular because both the Na^+ and NH_3^+ sites can be hydrated.

Parallel results have been obtained by Williams and coworkers who used BIRD to study the $M^+(Val)(H_2O)_x$ complexes where $M^+ = Li^+$, Na^+, and K^+ and x = 1 – 6.[126-128]

Alkali Metal Cations Interacting With Aliphatic Amino Acids

Sodium

We have acquired IRMPD spectra of the sodiated aliphatic amino acids: Gly, alanine (Ala), valine (Val), leucine (Leu), and isoleucine (Ile).[129] The spectra are similar except a band near 1400 cm^{-1} grows in for Ala – Ile. The similarity of the spectra indicates that the dominant isomer formed for all five complexes remains [N,CO], as noted above for Na^+(Gly). Notably, the addition of the side-chain leads to two [N,CO] isomers that differ in whether the sodium cation leans in the direction of the side-chain (lower in energy because of favorable electrostatics and designated as S for syn) or to the opposite side (designated as A for anti), Figure 3. The additional intensity near 1400 cm^{-1} was attributed to the zwitterionic [CO_2^-] isomer, which MP2 theory indicates lies less than 4 kJ/mol above the [N,CO] global minimum structure for Ala – Ile. Other levels of theory predict either too little of the zwitterionic structure (B3LYP-GD3BJ and M06-2X) or that it is dominant (B3LYP and B3P86), neither of which agrees with experiment.

TCID studies of these same complexes along with homo-alanine (hAla) find that the BDEs for Na^+-Xxx (Xxx = Gly, Ala, hAla, Val, Leu, Ile) systematically increase as the length of the side chain increases, with a span of 14 kJ/mol.[130] These BDEs are predicted well by B3LYP, B3P86, and MP2 levels of theory with B3LYP-GD3BJ and M06-2X yielding values that are too high. The increases correlate well with the polarizability of the aliphatic amino acids. Results obtained using the kinetic method[131, 132] and equilibrium methods[98] provide similar trends although the TCID data provide the best correlation with polarizability.

Potassium

TCID studies of the analogous six complexes with K^+ have also been performed.[120] Again the BDEs increase with increasing polarizability of the aliphatic amino acids, now over a range of 9 kJ/mol. This difference reflects the fact that the K^+(Xxx) BDEs are 73 ± 1% of the Na^+(Xxx) BDEs. Again B3LYP, B3P86, and MP2 levels of theory predict BDEs in good

agreement with experiment, whereas B3LYP-GD3BJ values are too high. Kinetic method results[133] are in reasonable agreement with the TCID results although slightly higher by an average of 2 ± 1 kJ/mol.

Cesium

Recent work has included IRMPD studies of the aliphatic amino acid complexes with Cs^+.[80] As noted above, this study examined the dichotomy of the [CO,OH] and [CO] double-well potential carefully for the Cs^+(Gly) system. As the side-chain is lengthened, the [CO] isomer becomes less stable at all levels of theory and, in particular, is essentially absent at the MP2 level. Thus, in all cases, the spectra can be assigned to a [CO,OH] isomer. In general, this corresponds to a specific orientation of the side chain, even though multiple possibilities exist, with the possible exception of hAla, where there are two low-lying [CO,OH] conformers. As for Cs^+(Gly), the B3LYP level of theory predicts IR spectra containing a band for the out-of-plane OH wag that does not match experiment. As noted above, if this band is red-shifted, as predicted by CCSD calculations for both Cs^+(Gly) and Cs^+(Ala), agreement between theory and experimental spectra is obtained.[80]

Effects of Hydration

The effects of adding water to M^+(Xxx) complexes have been studied by Williams and coworkers using kinetic data for $M^+(Val)(H_2O)_x$, x = 1 – 6 and M^+ = Li^+, Na^+, and K^+, [126, 127] BIRD measurements of the hydration energies for x = 1 – 3 for Li^+ and x = 1 for Na^+,[128, 134] and IRMPD spectroscopy for $Li^+(Val)(H_2O)_x$, x = 1 – 4.[135] Similar to Na^+(Gly) discussed above, the kinetic results indicate a change in metal cation coordination from [N,CO] to [CO,OH] at x = 3 for Li^+ and x = 2 for Na^+. IRMPD studies of $Li^+(Val)(H_2O)_x$ find the same result, but indicate clearly that this complex retains a charge-solvated [CO,OH] structure for x = 3 and 4, with no sign of a zwitterionic form suggested by the BIRD results.

Further measurements of the hydration energies of such complexes have been performed by Wincel using high-pressure equilibrium methods. His results include hydration energies for x = 1 – 3 of Na^+(Val)[100] (with good agreement with BIRD results for Val[134]) and of K^+(Xxx) where Xxx = Gly, Ala, and Val.[101]

Proline

TCID studies of lithiated, sodiated, and potassiated proline (Pro) find M^+(Pro) BDEs that match theory for the zwitterionic [CO_2^-] isomer.[67] Here, the zwitterionic isomer is favored because the secondary nitrogen in Pro makes it more acidic than the primary amino group in other amino acids. This study also considered the four- and six-membered ring analogues of the five-membered ring proline: azetidine-2-carboxylic acid (Aze) and pipecolic acid (Pip). Interestingly, the bonds to Pro are stronger than those to Aze and Pip for all three alkali cations, which is counter to expectations based on polarizability, where Pip is higher than Pro. Theory showed that this result occurs because the NH•••OC hydrogen bond is shorter in the complexes with Pro with no distortion to the ring.

The zwitterionic structure for the M^+(Pro) complexes has been verified by IRMPD studies for all five alkali cations.[118, 136] However, for the heavier alkali cations, K^+, Rb^+, and Cs^+, there is spectroscopic evidence for the coexistence of the [CO,OH] structure as well.[102] In particular, a comparison of potassiated Pro, N-methyl Pro (which increases the basicity of the amino group, enhancing the zwitterionic stability), and N-methyl Pro methylester (which removes the possibility of the zwitterion) showed that both [CO_2^-] and [CO,OH] were present. Theory indicates that the [CO_2^-] isomer is the global minimum structure for all five alkali cations, but the [CO,OH] structure drops in relative energy as the metal cation size increases, dropping to only 1.8 kJ/mol for Cs^+. Thus, for K^+, Rb^+, and Cs^+, there is again a double-well potential that permits simultaneous occupation of both isomers for these M^+(Pro) systems.

This study[102] went on to consider N-methyl Ala, which also has a secondary nitrogen and therefore exhibits parallel trends to Pro with regard to the relative stabilities of the zwitterionic and [CO,OH] structure. It went on to computationally compare these results with those for other amino acids, showing that the periodic trends in stability of the M^+(Xxx) complexes were generally parallel, but that ligands containing a secondary amine (Pro, Arg, and N-methyl Ala) stabilized the zwitterionic form.

Effects of Hydrating Proline Complexes

Unlike Na^+(Gly), where hydration shifts the complexation site from [N,CO] to [CO,OH], hydration of Na^+(Pro) retains the zwitterionic [CO_2^-] binding site.[137] TCID measurements of

$Na^+(Pro)(H_2O)_x$ complexes where x = 1 – 4 again find that bond energies for loss of water and proline decline monotonically with increasing hydration: 66 ± 5, 45 ± 5, 30 ± 4, and 20 ± 6 kJ/mol, respectively . The experimental BDEs are reproduced reasonably well by theory except for the loss of Pro from the x = 4 complex. The hydration energies are slightly weaker (by ~10 kJ/mol) for the $Na^+(Pro)$ complex compared to $Na^+(Gly)$ because the Na^+-Pro bond is stronger than the Na^+-Gly bond. Here, hydration energies for $x = 1 – 3$ of $Na^+(Pro)(H_2O)_x$ are in reasonable agreement with those measured by Wincel.[100]

As for the $Na^+(Gly)(H_2O)_x$ system, the global minimum structures of the x = 2 – 4 complexes of $Na^+(Pro)(H_2O)_x$ have a water molecule bound to the Na^+ site with a hydrogen bond to one of the carboxylic acid oxygens, forming HOH•••O$^-$•••H$^+$N hydrogen bonds. At x = 4, both the Na^+ and NH_2^+ sites can be fully hydrated.

Alkali Metal Cations Interacting With Functionalized Amino Acids

Extensive IRMPD spectroscopic studies have been performed to elucidate the structures of metallated amino acids with functionalized side chains.[29, 47, 64, 80, 90, 91, 118, 119, 136, 138-154] Structures were generally assigned on the basis of comparison to computational spectra. Table 1 compiles the results of this work. As for Gly, the structures evolve as the metal ion changes. The higher charge density on Li^+, the smallest alkali metal cation, generally results in tridentate [N,CO,SC] structures. Here, the metal binds to the amino nitrogen and carbonyl oxygen of the backbone along with the heteroatom or aromatic ring of the side-chain (SC). This is illustrated for the oxygen side-chain of serine in Figure 6.

This structural motif is largely maintained for Na^+ although tryptophan (Trp) and glutamine (Gln) also exhibit bidentate structures where the metal binds only to the backbone carbonyl and the side-chain, [CO,SC]. The very basic amino acid, arginine, also switches to having predominantly a zwitterionic structure, [CO_2^-], although the tridentate species is still observed.

For the heavier and lower charge density alkali cations, K^+, Rb^+, and Cs^+, the tridentate [N,CO,SC] geometry often remains either the global minimum structure [serine (Ser), threonine (Thr), methionine (Met), phenylalanine (Phe), tyrosine (Tyr), asparagine (Asn)] or

is low-lying [cysteine (Cys), tryptophan (Trp), aspartic acid (Asp), glutamic acid (Glu), glutamine (Gln), lysine (Lys), histidine (His)]. However, these M^+(Xxx) complexes generally exhibit additional isomers. Bidentate [CO,SC] coordination is observed for Phe (with Rb^+ and Cs^+), Trp (where it is the global minimum structure for Rb^+ and Cs^+), Glu (with Cs^+), Gln, and His (where it is the global minimum structure for all three metal cations). Tridentate [CO,OH,SC] structures are also observed for Asn, Asp, Gln (where it is the global minimum structure with Cs^+), and Lys (where it is the global minimum structure for all three metal cations), possibly for Met.

With K^+, Rb^+, and Cs^+, the bidentate [CO,OH] structure is often observed for the reasons discussed above for Gly. The [CO,OH] isomer becomes the global minimum structure for Cys and is low in energy for Ser, Thr, and His. Cys and Met, as well as cesiated Ser and Thr, also exhibit the zwitterionic form of this complexation, [CO_2^-], which is the exclusive form for Arg because of the high basicity of the side-chain. As discussed above for Gly, the [CO,OH] and [CO_2^-] species differ only in whether the proton remains on the oxygen of the carboxylic acid [CO,OH] or has transferred to the amino group [CO_2^-], such that they lie in a double-well potential, Figure 4b. This coordination favors [CO_2^-] when the metal charge density is high (e.g., for Li^+, Na^+, and metal dications) and favors [CO,OH] when the metal charge density is low (Rb^+ and Cs^+).[64, 153] However, these zwitterionic [CO_2^-] structures are not observed for Li^+ and Na^+ because the [N,CO,SC] structures are much more strongly favored. The [CO_2^-] and accompanying [CO,OH] structures become competitive for Rb^+ and Cs^+ (and sometimes K^+). Because the frequency of the proton motion that couples these two isomers is relatively high, the wavefunction associated with the ground vibrational level can sample both [CO_2^-] and [CO,OH] potential wells. In some cases, this has permitted the simultaneous observation of the CO stretches characteristic of the carboxylate and carboxylic acid groups.[64, 150] Figure 2 shows this for the case of Cs^+(Ser), where bands associated with both [COOH] and [CO_2^-] structures are observed. Figure 7 shows this for the example of Cs^+(Lys), which exhibits both [CO,OH,SC] and [CO_2^-,SC] coordination.[120]

It is generally the case that structures found experimentally agree with the lowest energy geometries located computationally, although this prediction can vary with the level of

theory. In many of our results, the relative stabilities predicted by single-point energy calculations at the MP2 level were preferred compared to B3LYP results. The agreement between experiment and theory also presumes that all accessible conformations are properly located. For example, assignments for structures of K^+(Lys), Cs^+(Lys), and Cs^+(Glu) were revised after locating lower-energy tridentate [CO,OH,SC] conformations.[145, 146, 149, 150, 155] It can also occur that the ion source conditions influence which structures are observed, especially if higher-energy isomers are kinetically trapped.[156]

Effects of Hydration

We have examined the effects of hydration with one to four water molecules attached to the Na^+(Cys) complex.[157] The complex starts with the sodium ion bound in a [N,CO,SC] tridentate configuration. The first two waters attach directly to the sodium ion. Depending on the level of theory, it is nearly isoenergetic for Na^+ to shift to a [CO] binding mode with one water ligand bridging from Na^+ to the hydroxyl oxygen. The zwitterionic form of this complex is also nearly isoenergetic. These binding modes remain low in energy for addition of the third water molecule, which can bind to Na^+, $–NH_3^+$, or –OH with nearly equivalent BDEs. Addition of the fourth water ligand leads to complete solvation of the Na^+ and $–NH_3^+$ groups in a [$CO_2^–$] coordination geometry. Solvation is complete in part because there is a strong intramolecular S•••HN hydrogen bond. Overall, this means that the global minimum structures of Na^+(Cys)$(H_2O)_4$ and Na^+(Pro)$(H_2O)_4$ are similar, i.e., both are zwitterionic with complete solvent shells. Similar trends are expected for other amino acids with functionalized side chains. Indeed, in the limit of full solvation, such zwitterionic forms are expected.[158]

Comparison of the BDEs among the Na^+(Xxx)$(H_2O)_x$ complexes for Xxx = Gly, Pro, Cys shows that for x = 1 and 2, the hydration energies (Gly > Cys > Pro) vary inversely with the Na^+-Xxx bond energy, i.e., Gly < Cys < Pro. This trend changes for x = 3 and 4, where the hydration energies to the Cys complex are stronger than those to Gly (by ~ 3 kJ/mol), which are stronger than those to Pro (by ~10 kJ/mol). This directly reflects the change in coordination noted above.

Additional hydration studies include the first and second hydration energies of Li^+(Gln) and Na^+(Gln)[159, 160] and the first hydration energies of Li^+(Lys)[161] obtained using BIRD.

Here, hydration does not affect the coordination of these metal cations to the amino acid, which retains the tridentate [N,CO,SC] structures. In contrast, according to IRMPD results, addition of a single water molecule to $M^+(Arg)(H_2O)$, where $M^+ = Li^+$ and Na^+, changes the coordination of Li^+ from tridentate [N,CO,SC] to zwitterionic [N,CO^-] coordination, whereas Na^+ maintains a zwitterionic [CO_2^-] structure.[151] Associated kinetic studies indicated that a second water ligand is likely to bind to the metal cation and a third to the cationic guanidinium side chain.

Further measurements of the hydration energies of such complexes have been performed by Wincel using high-pressure equilibrium methods. His results include hydration energies for $x = 1 - 3$ of Na^+(Xxx) where Xxx = Met, Phe, and Gln.[100] Here, good agreement with BIRD results for Gln. He has also examined K^+(Xxx) where Xxx = Gly, Ala, Val, Met, Pro, and Phe.[101]

Periodic Trends

A comprehensive listing of the known M^+–Xxx BDEs measured by TCID is given in Table 2.[25, 29, 47, 67, 85, 116, 117, 142, 143, 146, 150, 162-168] For completeness, a value obtained using the kinetic method is included for Na^+–Arg, where there is no TCID result.[169] For all amino acids, experimental and theoretical results for M^+(Xxx) BDEs decrease down the periodic table, $Li^+ > Na^+ > K^+ > Rb^+ > Cs^+$. As discussed above, this is primarily a reflection of the increasing radius of the metal cation: 0.70, 0.98, 1.33, 1.49, and 1.69 Å, respectively.[170] As the cation radius increases, the M^+–Xxx bond distances necessarily increase, which reduces the electrostatic interactions. Quantitatively, although there are clearly some variations, we find that relative to Na^+(Xxx) complexes, the BDEs for the analogous complexes with Li^+, K^+, Rb^+, and Cs^+ are 144 ± 11%, 74 ± 3%, 56 ± 21%, and 46 ± 21%, respectively.

Experimentally, we have found that the BDEs decrease approximately linearly with the inverse of the ionic radius, as shown in Figure 5 for Xxx = Gly, Pro, and Gln. Other amino acids have shown similar trends. At long range, the metal ion ligand interactions should comprise combinations of ion-dipole, ion-quadrupole, and ion-induced dipole forces, which change with interaction distance as r^{-2}, r^{-3}, and r^{-4}, respectively. The experimentally observed r^{-1} dependence suggests that strong electrostatic effects along with complex chelation effects

dominate at short range. The regression lines shown in Figure 5 for M^+ complexes of Gly, Pro, and Gln have slopes of 158 ± 6, 190 ± 8, and 214 ± 15 Å kJ/mol, respectively. These values accurately indicate the relative strengths of the interactions of different amino acids with the metal cations. Gly is the weakest binding amino acid and Gln is among the strongest binding amino acids measured to date, Table 2.

Effects of Polarizability and Side Chain on M^+(Xxx) BDEs.

A number of factors contribute to how the BDEs of alkali cations bound to amino acids vary with the side chain. Ruan and Rodgers showed that the bond energies of sodium and potassium ions to Gly and the aromatic amino acids, Phe, Tyr, and Trp, correlate well with the polarizabilities of the amino acids.[142] (It has been demonstrated that isotropic molecular polarizabilities calculated at the PBE0/6-311+G(2d,2p) level of theory using B3LYP/6-311G(d,p) optimized geometries provide values that agree well with measurements.[96] The polarizabilities used here for the neutral amino acid in the metal cationized complexes have been calculated at this level.) Rodgers and Armentrout extended that correlation to include Cys, Pro, and Met, as shown in Figure 8,[1] where the lines are regression analysis of the data for those seven amino acid complexes. They later showed that a similar correlation also holds for rubidium and cesium cation affinities,[143] where the latter is also included in Figure 8.

Subsequent work has demonstrated that polar side chains of Ser, Thr, Asp, Asn, Glu, Gln, Lys, and His all enhance the bonding further, Figure 8.[29, 47, 143, 146, 150, 163, 165, 168, 171] For Na^+ and K^+, BDEs to Ser, Thr, Asn, Gln, Lys, and His form a series that is parallel to those for the aliphatic and aromatic amino acids, with an average enhancement of approximately 28 and 24 kJ/mol, respectively.[163, 165] The acidic amino acids, Asp and Glu, show enhancements of ~15 kJ/mol, which lie in between the polar and aromatic series. The difference between Asp and Glu versus Asn and Gln demonstrates a lower binding energy for the carboxylic acid side-chain relative to the carboxamide side chain, which we attribute to an inductive effect of the hydroxyl group, as noted above. Further, Glu and Gln bind more tightly than Asp and Asn, respectively, in part because of the slightly higher polarizabilities, but also because the longer side chain in the former amino acids allows more flexibility in the orientation of the

side-chain binding site, as discussed further below.

The magnitude of these side-chain enhancements is partially related to the local dipole moment of the side-chain coordinating site, which can be quantified by comparing to molecules similar to the isolated side chains. For instance, acetamide (mimicking Asn and Gln) and imidazole (the side chain of His) have dipole moments of 3.68 and 3.8 D, whereas the 1.70 D dipole moment of acetic acid (Asp and Glu) is about half as large.[172] Methanol (mimicking Ser and Thr) also has a dipole of 1.70 D, but the enhancement is more like those of Asn, Gln, and His. We interpret this to indicate that the side-chain enhancements are influenced by the magnitude of the dipole along with how well the metal cation aligns with the dipole. This alignment can be influenced by the length of the side-chain, with effects described further below.

As the metal cation increases in size, these polar enhancements decrease not only because of the direct electrostatic effect on the bond length described above but also because the different lengths of the side chains influence whether the side chains can coordinate effectively. Thus, Ser and Thr, where the side chains are only two atoms long, have enhancements of 28, 24, 10, and 7 kJ/mol for Na^+, K^+, Rb^+, and Cs^+. Here, the larger metal cations are not able to bind as efficiently in a tridentate conformation as smaller cations.[25, 164] For Asp, Glu, and His, which have three, four, and three atom long side chains, the enhancements drop from 28 kJ/mol for Na^+ to 24 kJ/mol for K^+ to 15 kJ/mol for Rb^+ and Cs^+.[163] Thus, the longer side chains retain better tridentate binding than the shorter side chains. Likewise, Asn and Gln with 3- and 4-atom carboxamide side chains show trends of 28 and 28 kJ/mol for Na^+, 24 and 24 kJ/mol for K^+, 24 and 24 kJ/mol for Rb^+, and 15 and 24 kJ/mol for Cs^+.[146] These longer side chain lengths coupled with the strong binding carbonyl of the carboxamide group allow the enhancement to be nearly independent of metal cation for Gln and nearly so for Asn. Lys with its five-atom long side chain is even more flexible and also retains a relatively strong enhancement relative to the polarizability trend of 25 kJ/mol for Na^+, 18 kJ/mol for K^+, 20 kJ/mol for Rb^+, and 21 kJ/mol for Cs^+.[150] These enhancements are only ~4 kJ/mol weaker than those for Gln, which is somewhat surprising because the local dipole moment of the carboxamide group (estimated from acetamide, 3.68 D) is much

larger than that for the amine (estimated from methyl amine, 1.31 D).[172] The near equivalency suggests that the shorter side-chain length of Gln leads to some constraints on the binding distance and orientation of the side-chain group, whereas the more flexible lysine side-chain allows binding close to an optimum distance and orientation.

Given these observations regarding the effects of polarizability, local dipole of the side chain, and side-chain length, the trends in Table 1 become clearer. Alkali metal cations prefer to bind to the carbonyl group of any amino acid. Smaller cations prefer binding to the amino group and enhance these interactions by binding to the side chain, [N,CO,SC]. As the metal cation gets larger, the preference for the [N,CO,SC] isomers becomes comparable to that for [CO,OH,SC] and [CO,OH] isomers. Larger metal cations are also not able to bind as strongly to all three functional groups in tridentate structures, making the bidentate [CO,SC] structure competitive.

Alkali Metal Cations Interacting With Small Peptides

Small Peptides of Aliphatic Amino Acids

The simplest peptides, di- and tri-glycine (GG and GGG), complexed with sodium cations have been examined using theory, IRMPD spectroscopy,[27, 173] along with TCID[27, 174] and kinetic method measurements of the thermochemistry.[175] IRMPD results indicate that the sodium cation coordinates with the carbonyl groups but leaves open whether the N-terminal amino group is also coordinated. Theory indicates that both structures have relatively low energies, both for the sodiated and potassiated di- and tri-glycine.[27] Thus, in M^+(GG), the metal cations prefer bidentate [CO,CO] or tridentate [N,CO,CO] configurations, tridentate [CO,CO,CO] configurations in M^+(GGG), and [CO,CO,CO,CO] or [N,CO,CO,CO,CO] structures in M^+(GGGG). Similar spectroscopic results have been obtained for complexes of Li^+, Na^+, K^+, and Cs^+ with di- and tri-alanine.[173, 176-178]

TCID results are available only for sodium and potassium cations bound to GG and GGG, Table 2.[27, 174] The BDEs for these two sodiated systems agree well with results from the kinetic method, Figure 9, which includes GGGG as well as many other di- and tripeptides.[175] The experimental BDEs also agree reasonably well with theoretical values.[27,

[175, 179-182] As with all other ligands, the Na^+ affinities of these small peptides are greater than the K^+ affinities. Also as expected on the basis of increasing polarizability and available CO coordinating groups, the BDEs for both sodiated and potassiated G, GG, GGG, and GGGG increase with the size of the peptide, Figure 9. Notably, the increasing BDE with increasing residues begins to level off at GGGG, which suggests that the binding energies are limited by increased steric effects and decreasing charge density on Na^+ as the coordination number increases.[1] Clearly, as the coordination number saturates, no further increases can occur no matter how large the peptide may be.

Interestingly, the correlation with polarizability for the BDEs of G, GG, GGG, and GGGG, Figure 9, is not the same as that shown in Figure 8. This can be illustrated by comparing the BDEs of GG and Asn, which are isomers of one another and therefore have similar polarizabilities. These BDEs are the same within experimental uncertainty, such that GG shows an "enhanced" BDE similar to Asn, and therefore does not lie on the regression line of Figure 8 (dashed lines). Presumably, the additional CO coordination afforded by the additional residue again leads to coordinating carbonyl sites with an appreciable local dipole moment. Indeed, theory does find that the local dipole moments of the peptides are aligned with the metal ion in these complexes;[27, 182] however, the overall dipole moments of G, GG, and GGG in the geometries of the global minimum complexes (3.2, 5.8, and 5.2 D for Na^+, respectively, and 6.2, 5.9, and 7.8 D for K^+, respectively[27]) do not correlate directly with the increase in the experimental BDEs. We believe that this shows there is a complex superposition of electrostatic and steric effects that control the cation affinities of complex species like peptides.

Peptides with Functionalized Side Chains

When functionalized side chains are present, as for the isolated amino acids, the side chain will also participate in metal coordination. IRMPD results demonstrate that Na^+ and K^+ coordinate with PheAla and AlaPhe in either a [CO,CO,SC] or [N,CO,SC] geometry[183] and K^+(HisGly) favors an apparent [CO,CO,SC] geometry.[184] Likewise, the PhePhe dipeptide shows similar coordination for Li^+, Na^+, K^+, and Cs^+ complexes, with more strongly bound alkaline earth dications shifting to an intercalating [CO,CO,SC,SC] coordination.[185]

Potassium cation complexes with AlaAla, PheAla, PhePhe, AlaAlaAla, and PheGlyGly have similar IRMPD spectra that indicate CO and NH_2 coordination.[178]

When the side chain has a stronger interaction, unlike the cases noted above, inversion of the peptide sequence can have much larger effects.[186, 187] For example, M^+(GlyArg) where $M^+ = Li^+$, Na^+, and Cs^+ exhibit [CO,CO^-] coordination where there is a salt-bridge between the carboxylate anion and protonated guanidine side chain. This particular geometry has a nearly linear arrangement of formal charge sites that stabilizes this structure. In contrast, for M^+(ArgGly), the [CO,CO^-] salt-bridge geometry is retained for the larger K^+ and Cs^+ cations, but Li^+ exhibits [CO,CO,SC] coordination and Na^+ shows a mixture of both structures.

The thermochemistry for binding Na^+ to small peptides has been explored using the kinetic method.[175] Nineteen peptides containing 2 – 4 residues have been examined with BDEs that compared favorably to theoretical values. It was concluded that the coordination of Na^+ occurs to all available carbonyls in the most stable structure of the peptides but functionalized side chains also enhance the binding. For instance, the isomeric pairs of dipeptides (GlyPhe and PheGly, AlaTrp and TrpAla, and GlyHis and HisGly) show that the cation affinity is enhanced by 3 – 12 kJ/mol more when the functionalized side chain is at the N-terminus compared to the C-terminus.

Larger Peptides

In a few systems, the binding of alkali metal cations to larger peptides has been studied. IRMPD has been used to examine sodiated polyglycine (Gly_n) for $n = 2 – 8$.[173, 188, 189] As noted above, smaller peptides, $n = 2 – 5$, coordinate all carbonyl groups with the metal cation in globular structures. For the larger peptides beginning at $n = 6$, only six carbonyls can chelate the metal cation and the remaining parts of the peptide are stabilized by hydrogen bonding interactions, primarily between the termini. Experiments indicate that this hydrogen bonding interaction remains a charge-solvated (CS) structure, although theory indicates that the zwitterionic salt-bridge (SB) analogue (where a proton has transferred from the C-terminus to the N-terminus) becomes increasingly stabilized for n larger than 6. For example,

for $Na^+(G_7)$, the SB structure is calculated to lie 20 kJ/mol above the lowest CS structure, whereas for $Na^+(G_8)$, SB is calculated as 5.5 kJ/mol below the CS structure.[188, 189]

IRMPD studies of metallated pentaalanine (Ala_5) found that while Na^+ could bind five carbonyls, the larger K^+ and Cs^+ cations preferred structures with fewer coordinating carbonyls but stabilized by forming hydrogen bonds to the C-terminal carboxyl group.[190] Because these larger metal cations bind more weakly to the peptide, such intramolecular hydrogen bonding becomes thermodynamically competitive with the metal cation-peptide interactions, which influences the coordination.

The hydrogen bonding noted in these studies leads to the familiar α-helices and β-sheets found in the secondary structures of proteins. Indeed, IRMPD studies of $Na^+(Ala_n)$ complexes for n = 8 – 12 have examined the transition from the globular structures noted above to helical structures.[191] The octapeptide and nonapeptide spectra have features consistent with both globular and helical structures, whereas the larger oligopeptides transition to a helical form. This result differs somewhat from theory, which found that the helical form is the lowest in energy for all of these peptide complexes; however, the globular structures have relative free energies that make them accessible experimentally. The helical forms for the larger peptide complexes are also consistent with previous ion mobility measurements for $M^+(Ala_n)$ where n = 12 – 20 and M^+ = Li^+, Na^+, K^+, Rb^+, Cs^+.[192, 193] Although these experiments extended down to n = 6, ion mobility measurements cannot distinguish the globular and helical forms of these smaller peptides.

Group 12 Dications Interacting With Amino Acids and Peptides

Many metal dications bound to amino acids and small peptides have been examined using IRMPD spectroscopic techniques, for example.[194-210] This host of studies is beyond the scope of this perspective. Instead, we focus on our systematic studies of how zinc and its toxic congener, cadmium, interact with amino acids and small peptides using IRMPD action spectroscopy.[92-95, 211-220]

Our work was largely motivated by trying to understand the proclivity for divalent Zn^{2+} to bind to histidine (His) and cysteine (Cys) residues. These binding sites are found in

carbonic anhydrase, a metalloenzyme with zinc coordinated to three His residues, and in zinc finger proteins,[221-226] where zinc is usually coordinated with two His and two Cys residues, but one His and three Cys coordination has also been identified. Both motifs are associated with proteins that recognize, bind, and repair DNA and RNA.[225, 227] In finger proteins, the zinc ion can be substituted by toxic heavy metals like Cd^{2+}, even at low concentrations, which inhibits the functionality of the metalloprotein and can have a profound effect on the reproductive system, genomic stability, brain development, and tumor development.[227, 228] The carbonic anhydrase metalloenzyme seems less susceptible to deactivation when Zn^{2+} is replaced with Cd^{2+}.[229]

These systems have not been studied using TCID techniques. Although these complexes could undoubtedly be examined using this technique, because the ligand is deprotonated in many cases, it is unlikely that a simple bond cleavage to form the metal cation and ligand will occur.[195] Rather, more complex dissociation channels are likely, making the translation to quantitative metal-ligand bond energies difficult.

Amino acids

Table 3 includes a partial list of the amino acids studied and the geometries observed. Because Zn and Cd prefer a +2 oxidation state, when these complexes are formed by electrospray ionization, either the ligand is deprotonated, such that the $M(Xxx\text{-}H)^+$ complex is formed, or the anion (usually the chloride) in the salt used to supply the metal remains, giving the $MCl^+(Xxx)$ complex. In our studies of fifteen different amino acids, the former complex is generally formed (all but three) for zinc, whereas cadmium generally yields the chloride complexes, Table 3. In most circumstances, the complexes are tridentate, interacting with the amino group nitrogen, the carbonyl, and the side chain heteroatom or aromatic ring. When deprotonated, the carboxylic acid is usually the site of deprotonation. Exceptions where the side chain is deprotonated instead include Ser, Thr (minor component), Cys and its methyl ester (where the Cd analogue is also formed). The ability of the thiol side chain of Cys to deprotonate easily is probably one of the reasons that Cys residues are a common binding site for Zn in biological systems.

One particularly interesting case was the zinc complex of deprotonated aspartic acid (Asp).[214] The expected [N,CO^-,SC] structure of Zn(Asp-H)$^+$ was clearly found when an extra ligand (L) was attached, either acetonitrile or another intact Asp, Figure 10a; however, the IRMPD spectrum of the bare Zn(Asp-H)$^+$ complex was just as clearly not this structure. Instead, this complex had rearranged by eliminating ammonia to generate the isobaric Zn(Asp-NH_3)$^+$[CO_2^-,SC](NH_3) complex, Figure 10b. Theory showed that this rearranged species is much lower in energy (by 70 – 90 kJ/mol) than the intact Zn(Asp-H)$^+$ complex. In retrospect, it was shown that the comparable Zn(Asn-H)$^+$ complex had also undergone ammonia loss, although to a much smaller extent than Asp. Another interesting case like this has been shown for Zn(Pro-H)$^+$ by Fridgen and coworkers.[205] This complex rearranges by transferring a hydrogen from the C_2 or C_5 carbon to the zinc center, forming a HZn(Pro-2H)$^+$ complex where the zinc binds to the carbonyl oxygen and nitrogen.

In the Zn^+(Asp-H)(Asp) complex alluded to above, the deprotonated aspartic acid binds in the expected [N,CO^-,SC] tridentate manner, and the intact Asp similarly binds tridentate as [N,CO,SC].[214] In contrast, when there are two His ligands, more variations are observed for both Zn and Cd complexes. When one of the ligands is deprotonated, M^+(His-H)(His), the major structure observed is tridentate for the deprotonated ligand, [N,CO^-,SC], where the carboxylic acid is anionic, Figure 11.[217] The intact His ligand is zwitterionic because the proton has been transferred from the carboxlic acid to the N_π nitrogen on the His sidechain, with the metal bound to [CO_2^-]. The two ligands are bound together via a CO^-•••HN_π hydrogen bond, Figure 11. A minor structure of [N,CO^-,SC][N,SC] was also identified where the intact His ligand is now charge-solvated and the metal binds to the amine nitrogen and N_π nitrogen of the side chain.

Uniquely among the amino acids we have studied, we also observed M^{2+}(His)$_2$ complexes for both Zn and Cd, where no deprotonation occurred.[211] The uniqueness of observing this dimer species among all the amino acids studied seems aligned with the proclivity of Zn to bind to His residues. In the major structure observed, both ligands are charge solvated [N,CO,SC][N,CO,SC], Figure 11, but bands indicative of a zwitterionic

ligand are also observed, likely associated with [N,CO,SC][CO_2^-] coordination where a proton transfer from CO_2H to N_π has occurred.

Peptides

To date, we have studied few small peptides bound to Zn and Cd using IRMPD. The first was the HisHis dipeptide.[220] Here, coordination with the N_π nitrogen on the sidechain is dominant with Zn and Cd: [SC,N_i,SC,CO] coordination found for M^{2+}(HisHis) for both metals (shown in Figure 11 for Zn) along with a small population of [N,SC,N_i,SC] for Zn. Here, N_i refers to an iminol nitrogen, a coordination type first identified by Dunbar et al.,[209] where the hydrogen on a backbone amide nitrogen has migrated to a carbonyl oxygen, thereby providing a strong binding site (N_i) for the metal cation. Our IRMPD work also included M = Cu and found unique coordination compared to Zn and Cd, [N,SC,N_i,CO], where the iminol hydrogen has further migrated to the second side-chain N_π, forming a CO•••HN_π hydrogen bond.[220] The fact that Cu binds to only one of the His sidechains whereas Zn and Cd bind to two may be another indication of metal specificity for the His residue.

It is interesting to compare this coordination with that found for M^+(His-H)(His), where [N,CO^-,SC][CO_2^-] coordination was found, and $M^{2+}(His)_2$, where the major geometry observed was [N,CO,SC][N,CO,SC] (see above), Figure 11. Note that in all these complexes, coordination to the His side chain is favored, but the dipeptide restricts the coordination number to four compared to five or six for the His dimers. By linking the two amino acids with a peptide bond, the possible coordination is now sterically more restricted compared to two separate amino acid ligands that are free to orient in favorable positions. In addition, the free amino acids can utilize the C-terminus as a binding site, which is generally unavailable in proteins. Such distinctions need to be kept in mind when extrapolating such biomimetic studies to understand the binding sites in zinc finger proteins.

In ongoing work, we have also studied the coordination of Zn^{2+} and Cd^{2+} with a series of tripeptides containing His, differentiated by their position in the peptide: HisAlaAla, AlaHisAla, and AlaAlaHis.[230] IRMPD results for the Zn and Cd complexes indicate that when the histidine residue is located at the N-terminus (HAA), the dominant conformation

observed is [N,SC,CO,CO,CO]. In contrast, when histidine is the central residue (AHA), an iminol conformer, [N,N_i,SC,N_i,CO], is preferred.[209] It seems feasible that in the condensed phase, similar interactions might be facilitated by proton transfer to the surrounding solvent or nearby acidic residues. The iminol motif is also important when His is located at the C-terminus (AAH). For the Zn^{2+}(AAH) complex, an iminol structure [N,N_i,N_i,CO,SC] dominates along with some population of [N,CO,CO,SC]. For the larger Cd dication, the latter structure dominates but the former is also clearly present. Again, the His side chain is involved in the coordination in all cases, but the preference for the iminol motif varies with the location of the His residue.

These results for Zn^{2+} and Cd^{2+} can also be compared with the IRMPD studies of Dunbar et al. on Ni^{2+} and Cu^{2+} complexes of the same three peptides.[209]Here, iminol structures dominated the observed spectra, but for these metals, coordination was generally limited to a four-coordinate square-planar geometry. This is presumably a result of the open-shell character of these metals compared with the closed-shell d^{10} configurations on Zn^{2+} and Cd^{2+}.

Conclusion And Future Directions

In this perspective, results from two distinct types of gas-phase studies have been explored. Threshold collision-induced (TCID) dissociation studies utilizing a guided ion beam tandem mass spectrometer (GIBMS) can provide thermodynamic information regarding the interactions of metal cations with amino acids and peptides, as well as other biological molecules not included here. Infrared multiple photon dissociation (IRMPD) action spectroscopy can determine the IR spectrum of such metal-ligand complexes, thereby providing structural information. Both approaches benefit from a close collaboration with theory to explore conformational space and determine details of the metal-ligand interactions. These comparisons benefit from the fact that the experimental results can be directly compared with computational results without the need to consider the solvent or substrate environment. Overall, the combination of TCID, IRMPD, and theory can provide considerable detail regarding how metal cations interact with biological systems ranging in

size from simple model compounds up to peptides and through the constituents of proteins. By looking at the trends in these model systems, factors that are important in determining the strength of metal cation interactions with biological molecules can be identified and quantified. Trends explored here include the metal identity and its size (illustrated in Figure 5), polarizabilities, local dipole moments, and side-chain lengths of the ligands (all illustrated in Figure 8), the length of the peptide (shown in Figure 9), and the effects of increasing hydration. The fundamental aspects of these pairwise interactions certainly extend to more complicated systems and the trends help transcend the biomimetic aspects of these studies. Further, more subtle aspects of these interactions (such as those illustrated in Figure 4) can also be explored quantitatively in the smaller systems explored here but reveal factors that should still be important as their size increases.

Nevertheless, the examination of these smaller model systems means that some projection is needed to apply these findings to real biological systems. Continued research is exploring ever larger complexes that should begin to bridge the gap between the small molecule chemistry reviewed here and functional biological molecules. One anticipates that such studies should allow lessons learned from smaller model systems to translate even more effectively to larger complex systems and to provide direct quantitative information about how secondary structure influences their properties and function.

Conflicts of Interest

There are no conflicts of interest to declare.

Acknowledgment: Many students and collaborators have contributed to the work described here, including reading through the present manuscript, and I thank them profusely. I also appreciate the insightful suggestions of both reviewers and several of my students. The research discussed here has been supported by the National Science Foundation, presently Grant CHE-2313553.

References

1. Rodgers, M. T.; Armentrout, P. B. A Thermodynamic "Vocabulary" for Metal Ion Interactions in Biological Systems. *Acc. Chem. Res.* **2004,** *37*, 989-998.
2. Rajabi, K.; Gillis, E. A. L.; Fridgen, T. D. Structures of Alkali Metal Ion−Adenine Complexes and Hydrated Complexes by IRMPD Spectroscopy and Electronic Structure Calculations. *J. Phys. Chem. A* **2010,** *114*, 3449-3456.
3. Yang, B.; Wu, R. R.; Polfer, N. C.; Berden, G.; Oomens, J.; Rodgers, M. T. IRMPD Action Spectroscopy of Alkali Metal Cation–Cytosine Complexes: Effects of Alkali Metal Cation Size on Gas Phase Conformation. *J. Am. Soc. Mass Spectrom.* **2013,** *24*, 1523-1533.
4. Gillis, E. A. L.; Rajabi, K.; Fridgen, T. D. Structures of Hydrated Li^+−Thymine and Li^+−Uracil Complexes by IRMPD Spectroscopy in the N−H/O−H Stretching Region. *J. Phys. Chem. A* **2009,** *113*, 824-832.
5. Nei, Y.-w.; Akinyemi, T. E.; Kaczan, C. M.; Steill, J. D.; Berden, G.; Oomens, J.; Rodgers, M. T. Infrared multiple photon dissociation action spectroscopy of sodiated uracil and thiouracils: Effects of thioketo-substitution on gas-phase conformation. *Int. J. Mass Spectrom.* **2011,** *308*, 191-202.
6. Kaczan, C. M.; Rathur, A. I.; Wu, R. R.; Chen, Y.; Austin, C. A.; Berden, G.; Oomens, J.; Rodgers, M. T. Infrared multiple photon dissociation action spectroscopy of sodium cationized halouracils: Effects of sodium cationization and halogenation on gas-phase conformation. *Int. J. Mass Spectrom.* **2015,** *378*, 76-85.
7. Shammel Baker, E.; Gidden, J.; Ferzoco, A.; Bowers, M. T. Sodium stabilization of dinucleotide multiplexes in the gas phase. *Phys. Chem. Chem. Phys.* **2004,** *6*, 2786-2795.
8. Rodgers, M. T.; Armentrout, P. B. Noncovalent Interactions of Nucleic Acid Bases (Uracil, Thymine, and Adenine) with Alkali Metal Ions. Threshold Collision-Induced Dissociation and Theoretical Studies. *J. Am. Chem. Soc.* **2000,** *122*, 8548-8558.
9. Cerda, B. A.; Wesdemiotis, C. Li^+, Na^+, and K^+ binding to the DNA and RNA nucleobases. Bond energies and attachment sites from the dissociation of metal ion-bound heterodimers. *J. Am. Chem. Soc.* **1996,** *118*, 11884-11892.
10. Yang, B.; Rodgers, M. T. Alkali metal cation binding affinities of cytosine in the gas phase: revisited. *Phys. Chem. Chem. Phys.* **2014,** *16*, 16110-16120.
11. Wang, P.; Polce, M. J.; Ohanessian, G.; Wesdemiotis, C. The sodium ion affinities of cytosine and its methylated derivatives. *J. Mass Spectrom.* **2008,** *43*, 485-494.
12. Yang, Z.; Rodgers, M. T. Tautomerization in the Formation and Collision-Induced Dissociation of Alkali Metal Cation-Cytosine Complexes. *Phys. Chem. Chem. Phys.* **2012,** *14*, 4517-4526.
13. Lehninger, A. L., *Biochemistry, The Molecular Basis of Cell Structure and Function*. 2nd ed.; Worth Publishers, Inc.: New York, 1977.
14. Yang, Z.; Rodgers, M. T. Influence of Halogenation on the Properties of Uracil and Its Noncovalent Interactions with Alkali Metal Ions. Threshold Collision-Induced Dissociation and Theoretical Studies. *J. Am. Chem. Soc.* **2004,** *126*, 16217-16226.
15. Yang, Z.; Rodgers, M. T. Influence of Thioketo Substitution on the Properties of Uracil and Its Noncovalent Interactions with Alkali Metal Ions: Threshold Collision-Induced Dissociation and Theoretical Studies. *J. Phys. Chem. A* **2006,** *110*, 1455-1468.
16. Wincel, H. Gas-Phase Hydration Thermochemistry of Sodiated and Potassiated Nucleic Acid Bases. *J. Am. Soc. Mass Spectrom.* **2012,** *23*, 1479-1487.

17. Wincel, H. Hydration Energies of Protonated and Sodiated Thiouracils. *J. Am. Soc. Mass Spectrom.* **2014,** *25*, 2134-2142.
18. Papayannopoulos, I. A. The interpretation of collision-induced dissociation tandem mass spectra of peptides. *Mass Spectrom. Rev.* **1995,** *14*, 49-73.
19. Armentrout, P. B. Not Just a Structural Tool: The Use of Guided Ion Beam Tandem Mass Spectrometry to Determine Thermochemistry. *J. Am. Soc. Mass Spectrom.* **2002,** *13*, 419-434.
20. Armentrout, P. B., Thermochemical Measurements by Guided Ion Beam Mass Spectrometry. In *Adv. Gas Phase Ion Chem.*, Adams, N.; Babcock, L. M., Eds. JAI Press: Greenwich, Connecticut, 1992; Vol. 1, pp 83-119.
21. Armentrout, P. B. The Kinetic Energy Dependence of Ion-Molecule Reactions: Guided Ion Beams and Threshold Measurements. *Int. J. Mass Spectrom.* **2000,** *200*, 219-241.
22. Armentrout, P. B., Threshold Collision-Induced Dissociations for the Determination of Accurate Gas-Phase Binding Energies and Reaction Barriers. In *Modern Mass Spectrometry*, Schalley, C., Ed. Springer-Verlag: Berlin, 2003; Vol. 225, pp 233-262.
23. Armentrout, P. B. The Power of Accurate Energetics (or Thermochemistry: What is it Good for?). *J. Am. Soc. Mass Spectrom.* **2013,** *24*, 173-185.
24. Ervin, K. M.; Armentrout, P. B. Translational Energy Dependence of $Ar^+ + XY \rightarrow ArX^+ + Y$ (XY = H_2, D_2, HD) from Thermal to 30 eV c.m. *J. Chem. Phys.* **1985,** *83*, 166-189.
25. Armentrout, P. B.; Chen, Y.; Rodgers, M. T. Metal Cation Dependence of Interactions with Amino Acids: Bond Energies of Cs^+ to Gly, Pro, Ser, Thr, and Cys. *J. Phys. Chem. A* **2012,** *116*, 3989-3999.
26. Moision, R. M.; Armentrout, P. B. An Electrospray Ionization Source for Thermochemical Investigation with the Guided Ion Beam Mass Spectrometer. *J. Am. Soc. Mass Spectrom.* **2007,** *18*, 1124-1134.
27. Ye, S. J.; Armentrout, P. B. Absolute Thermodynamic Measurements of Alkali Metal Cation Interactions with a Simple Dipeptide and Tripeptide. *J. Phys. Chem. A* **2008,** *112*, 3587-3596.
28. Heaton, A. L.; Armentrout, P. B. Thermodynamics and Mechanism of the Deamidation of Sodium-Bound Asparagine. *J. Am. Chem. Soc.* **2008,** *130*, 10227-10232.
29. Heaton, A. L.; Moision, R. M.; Armentrout, P. B. Experimental and Theoretical Studies of Sodium Cation Interactions with the Acidic Amino Acids and Their Amide Derivatives. *J. Phys. Chem. A* **2008,** *112*, 3319-3327.
30. Carpenter, J. E.; McNary, C. P.; Furin, A.; Sweeney, A. F.; Armentrout, P. B. How Hot are Your Ions Really? A Threshold Collision-Induced Dissociation Study of Substituted Benzylpyridinium "Thermometer" Ions. *J. Am. Soc. Mass Spectrom.* **2017,** *28*, 1876-1888.
31. Schultz, R. H.; Crellin, K. C.; Armentrout, P. B. Sequential Bond Energies of $Fe(CO)_x^+$ (x = 1 - 5): Systematic Effects on Collision-Induced Dissociation Measurements. *J. Am. Chem. Soc.* **1991,** *113*, 8590-8601.
32. Hales, D. A.; Lian, L.; Armentrout, P. B. Collision-Induced Dissociation of Nb_n^+ (n = 2 - 11): Bond Energies and Dissociation Pathways. *Int. J. Mass Spectrom. Ion Processes* **1990,** *102*, 269-301.
33. Rodgers, M. T.; Ervin, K. M.; Armentrout, P. B. Statistical Modeling of Collision-Induced Dissociation Thresholds. *J. Chem. Phys.* **1997,** *106*, 4499-4508.

34. Rodgers, M. T.; Armentrout, P. B. Statistical Modeling of Competitive Threshold Collision-Induced Dissociation. *J. Chem. Phys.* **1998,** *109*, 1787-1800.
35. Muntean, F.; Armentrout, P. B. Modeling kinetic shifts and competition in threshold collision-induced dissociation. Case study: *n*-butylbenzene cation dissociation. *J. Phys. Chem. A* **2003,** *107*, 7413-7422.
36. Muntean, F.; Heumann, L.; Armentrout, P. B. Modeling kinetic shifts in threshold collision-induced dissociation. Case study: dichlorobenzene cation dissociation. *J. Chem. Phys.* **2002,** *116*, 5593-5602.
37. Muntean, F.; Armentrout, P. B. Modeling Kinetic Shifts for Tight Transition States in Threshold Collision-Induced Dissociation. Case Study: Phenol Cation. *J. Phys. Chem. B* **2002,** *106*, 8117-8124.
38. Armentrout, P. B. Statistical modeling of sequential collision-induced dissociation. *J. Chem. Phys.* **2007,** *126*, 234302.
39. Armentrout, P. B.; Ervin, K. M.; Rodgers, M. T. Statistical Rate Theory and Kinetic Energy-Resolved Ion Chemistry – Theory and Applications. *J. Phys. Chem. A* **2008,** *112*, 10071-10085.
40. Dalleska, N. F.; Honma, K.; Armentrout, P. B. Stepwise Solvation Enthalpies of Protonated Water Clusters: Collision Induced Dissociation as an Alternative to Equilibrium Studies. *J. Am. Chem. Soc.* **1993,** *115*, 12125-12131.
41. Dalleska, N. F.; Honma, K.; Sunderlin, L. S.; Armentrout, P. B. Solvation of Transition Metal Ions by Water. Sequential Binding Energies of $M^+(H_2O)_x$ (x = 1 - 4) for M = Ti - Cu Determined by Collision-Induced Dissociation. *J. Am. Chem. Soc.* **1994,** *116*, 3519-3528.
42. Dalleska, N. F.; Tjelta, B. L.; Armentrout, P. B. Sequential Bond Energies of Water to Na^+ ($3s^0$), Mg^+($3s^1$), and Al^+ ($3s^2$). *J. Phys. Chem.* **1994,** *98*, 4191-4195.
43. Rodgers, M. T.; Armentrout, P. B. Collision-Induced Dissociation Measurements on $Li^+(H_2O)_n$, n = 1 - 6: The First Direct Measurement of the Li^+-OH_2 Bond Energy. *J. Phys. Chem. A* **1997,** *101*, 1238-1249.
44. Rodgers, M. T.; Armentrout, P. B. Absolute Binding Energies of Lithium Ions to Short Chain Alcohols, $C_nH_{n+2}O$, n = 1 - 4, Determined by Threshold Collision-Induced Dissociation. *J. Phys. Chem. A* **1997,** *101*, 2614-2625.
45. Iceman, C.; Armentrout, P. B. Collision-Induced Dissociation and Theoretical Studies of K^+ Complexes with Ammonia: A Test of Theory for Potassium Ions. *Int. J. Mass Spectrom.* **2003,** *222*, 329-349.
46. Amicangelo, J. C.; Armentrout, P. B. Ligand Exchange Reactions of Sodium Cation Complexes Examined Using Guided Ion Beam Mass Spectrometry: Relative and Absolute Dissociation Free Energies and Entropies. *J. Phys. Chem. A* **2004,** *108*, 10698-10713.
47. Heaton, A. L.; Armentrout, P. B. Experimental and Theoretical Studies of Potassium Cation Interactions with the Acidic Amino Acids and Their Amide Derivatives. *J. Phys. Chem. B* **2008,** *112*, 12056–12065.
48. Armentrout, P. B.; Heaton, A. L. Thermodynamics and Mechanisms of Protonated Diglycine Decomposition: A Guided Ion Beam Study. *J. Am. Soc. Mass Spectrom.* **2012,** *23*, 632-643.
49. Armentrout, P. B.; Stennett, E. M. S. Thermodynamics and Mechanism of Protonated Cysteine Decomposition: A Guided Ion Beam and Computational Study. *J. Am. Soc. Mass Spectrom.* **2014,** *25*, 512-523.

50. Mookherjee, A.; Van Stipdonk, M. J.; Armentrout, P. B. Thermodynamics and Reaction Mechanisms of Decomposition of the Simplest Protonated Tripeptide, Triglycine: A Guided Ion Beam and Computational Study. *J. Am Soc. Mass Spectrom.* **2017,** *28*, 739-757.
51. Mookherjee, A.; Armentrout, P. B. Thermodynamics and Reaction Mechanisms for Decomposition of a Simple Protonated Tripeptide, H^+GAG: a Guided Ion Beam and Computational Study. *J. Am. Soc. Mass Spectrom.* **2019,** *30*, 1013-1027.
52. Jones, R. M.; Boles, G. C.; Armentrout, P. B. Cis-trans isomerization is not rate determining for b_2 ion structures: A guided ion beam and computational study of the decomposition of H^+(GlyProAla). *Int. J. Mass Spectrom.* **2020,** *458*, 116434.
53. Mookherjee, A.; Armentrout, P. B. Thermodynamics and Reaction Mechanisms for Decomposition of a Simple Protonated Tripeptide, H^+GGA: From H^+GGG to H^+GAG to H^+GGA. *J. Am. Soc. Mass Spectrom.* **2022,** *33*, 355-368.
54. Heaton, A. L.; Ye, S. J.; Armentrout, P. B. Experimental and Theoretical Studies of Sodium Cation Complexes of the Deamidation and Dehydration Products of Asparagine, Glutamine, Aspartic Acid, and Glutamic Acid. *J. Phys. Chem. A* **2008,** *112*, 3328-3338.
55. Ye, S. J.; Armentrout, P. B. An Experimental and Theoretical Investigation of the Decomposition of Lithiated Hydroxyl Side Chain Amino Acids. *J. Phys. Chem. B* **2008,** *112*, 10303-10313.
56. Armentrout, P. B.; Clark, A. A. The Simplest b_2^+ Ion: Determining Its Structure from Its Energetics by a Direct Comparison of the Threshold Collision-induced Dissociation of Protonated Oxazolone and Diketopiperazine. *Int. J. Mass Spectrom.* **2012,** *316-318*, 182–191.
57. Kamrath, M. Z.; Garand, E.; Jordan, P. A.; Leavitt, C. M.; Wolk, A. B.; Van Stipdonk, M. J.; Miller, S. J.; Johnson, M. A. Vibrational Characterization of Simple Peptides Using Cryogenic Infrared Photodissociation of H2-Tagged, Mass-Selected Ions. *J. Am. Chem. Soc.* **2011,** *133*, 6440-6448.
58. Polfer, N. C.; Oomens, J. Reaction products in mass spectrometry elucidated with infrared spectroscopy. *Phys. Chem. Chem. Phys.* **2007,** *9*, 3804-3817.
59. Martens, J.; van Outersterp, R. E.; Vreeken, R. J.; Cuyckens, F.; Coene, K. L. M.; Engelke, U. F.; Kluijtmans, L. A. J.; Wevers, R. A.; Buydens, L. M. C.; Redlich, B., et al. Infrared ion spectroscopy: New opportunities for small-molecule identification in mass spectrometry - A tutorial perspective. *Anal. Chim. Acta* **2020,** *1093*, 1-15.
60. Lehmann, K. K.; Scoles, G.; Pate, B. H. Intramolecular Dynamics from Eigenstate-Resolved Infrared-Spectra. *Annu. Rev. Phys. Chem.* **1994,** *45*, 241−274.
61. Beil, A.; Luckhaus, D.; Quack, M.; Stohner, J. Intramolecular Vibrational Redistribution and Unimolecular Reaction: Concepts and New Results on the Femtosecond Dynamics and Statistics in CHBrClF. *Ber. Bunsen Phys. Chem.* **1997,** *101*, 311−328.
62. Black, J. G.; Yablonovitch, E.; Bloembergen, N.; Mukamel, S. Collisionless Multiphoton Dissociation of SF6: A Statistical Thermodynamic Process. *Phys. Rev. Lett.* **1977,** *38*, 1131−1134.
63. Grant, E.; Schulz, P.; Sudbo, A. S.; Shen, Y.; Lee, Y. T. Is Multiphoton Dissociation of Molecules a Statistical Thermal Process? *Phys. Rev. Lett.* **1978,** *40*, 115−118.
64. Armentrout, P. B.; Rodgers, M. T.; Oomens, J.; Steill, J. D. Infrared Multiphoton Dissociation Spectroscopy of Cationized Serine: Effects of Alkali-Metal Cation Size on Gas-Phase Conformation. *J. Phys. Chem. A* **2008,** *112*, 2248-2257.

65. Frisch, M. J.; Trucks, G. W.; Schlegel, H. B.; Scuseria, G. E.; Robb, M. A.; Cheeseman, J. R.; Scalmani, G.; Barone, V.; Petersson, G. A.; Nakatsuji, H., et al. *Gaussian 16, Revision A.03*, Gaussian, Inc.: Wallingford CT, 2016.
66. Leininger, T.; Nicklass, A.; Kuechle, W.; Stoll, H.; Dolg, M.; Bergner, A. The Accuracy of the Pseudopotential Approximation: Non-Frozen-Core Effects for Spectroscopic Constants of Alkali Fluorides XF (X = K, Rb, Cs). *Chem. Phys. Lett.* **1996,** *255*, 274-280.
67. Moision, R. M.; Armentrout, P. B. The Special Five-membered Ring of Proline: An Experimental and Theoretical Investigation of Alkali Metal Cation Interactions with Proline and Its Four- and Six-membered Ring Analogues. *J. Phys. Chem. A* **2006,** *110*, 3933-3946.
68. McNary, C. P.; Armentrout, P. B. Threshold Collision-Induced Dissociation of Proton-Bound Hydrazine and Dimethylhydrazine Clusters. *J. Phys. Chem. A* **2016,** *120*, 9690-9701.
69. McNary, C. P.; Nei, Y.-w.; Maitre, P.; Rodgers, M. T.; Armentrout, P. B. Infrared Multiple Photon Dissociation Spectroscopy of Protonated Glycine, Lysine, Histidine, and Arginine Complexed with 18-Crown-6. *Phys. Chem. Chem. Phys.* **2019,** *21*, 12625-12639.
70. Valiev, M.; Bylaska, E. J.; Govind, N.; Kowalski, K.; Straatsma, T. P.; Van Dam, H. J. J.; Wang, D.; Nieplocha, J.; Apra, E.; al., E. NWChem: A comprehensive and scalable open-source solution for large scale molecular simulations. *Comput. Phys. Commun.* **2010,** *181*, 1477-1489.
71. Case, D. A.; Babin, V.; Berryman, J. T.; Betz, R. M.; Cai, Q.; Cerutti, D. S.; Cheatham, T. E.; Darden, T. A.; Duke, R. E.; Gohlke, H., et al. *AMBER 14*, University of California: San Francisco, 2014.
72. Becke, A. D. Density-functional Thermochemistry. III. The Role of Exact Exchange. *J. Chem. Phys.* **1993,** *98*, 5648-5652.
73. Lee, C.; Yang, W.; Parr, R. G. Development of the Colle-Salvetti Correlation-Energy Formula into a Functional of the Electron Density. *Phys. Rev. B* **1988,** *37*, 785-789.
74. Grimme, S.; Antony, J.; Ehrlich, S.; Krieg, H. A Consistent and Accurate Ab Initio Parametrization of Density Functional Dispersion Correction (DFT-D) for the 94 Elements H-Pu. *J. Chem. Phys.* **2010,** *132*, 154104-154119.
75. Grimme, S.; Ehrlich, S.; Goerigk, L. Effect of the Damping Function in Dispersion Corrected Density Functional Theory. *J. Comput. Chem.* **2011,** *32*, 1456-1465.
76. Möller, C.; Plesset, M. S. Note on an Approximation Treatment for Many-Electron Systems. *Phys. Rev.* **1934,** *46*, 618-622.
77. Zhao, Y.; Truhlar, D. G. The M06 Suite of Density Functionals for Main Group Thermochemistry, Thermochemical Kinetics, Noncovalent Interactions, Excited States, and Transition Elements: Two New Functionals and Systematic Testing of Four M06-Class Functionals and 12 Other Functionals. *Theor. Chem. Acc.* **2008,** *120*, 215-241.
78. Purvis, G. D.; Bartlett, R. J. A Full Coupled-Cluster Singles and Doubles Model: The Inclusion of Disconnected Triples. *J. Chem. Phys.* **1982,** *76*, 1910-1918.
79. Scuseria, G. E.; Janssen, C. L.; Schaefer, H. F. An Efficient Reformulation Of The Closed-Shell Coupled Cluster Single And Double Excitation (CCSD) Equations. *J. Chem. Phys.* **1988,** *89*, 7382-7387.
80. Armentrout, P. B.; Steele, R. P.; Stevenson, B. C.; Jones, R. M.; Martens, J.; Berden, G.; Oomens, J. Infrared multiple photon dissociation spectra of cesiated complexes of the aliphatic amino acids: Challenges for conformational-space calculations by density functional theory. *Int. J. Mass Spectrom.* **2024,** *498*, 117201.

81. Mardirossian, N.; Head-Gordon, M. ωB97M-V: A combinatorially optimized, range-separated hybrid, meta-GGA density functional with VV10 nonlocal correlation. *J. Chem. Phys.* **2016,** *144*, 214110.
82. Kesharwani, M. K.; Brauer, B.; Martin, J. M. L. Frequency and Zero-Point Vibrational Energy Scale Factors for Double-Hybrid Density Functionals (and Other Selected Methods): Can Anharmonic Force Fields Be Avoided? *J. Phys. Chem. A* **2015,** *119*, 1701-1714.
83. Boys, S. F.; Bernardi, R. The Calculation of Small Molecular Interactions by the Differences of Separate Total Energies. Some Procedures with Reduced Errors. *Mol. Phys.* **1970,** *19*, 553-566.
84. van Duijneveldt, F. B.; van Duijneveldt-van de Rijdt, J. G. C. M.; van Lenthe, J. H. State of the Art in Counterpoise Theory. *Chem. Rev.* **1994,** *94*, 1873-1885.
85. Rodgers, M. T.; Armentrout, P. B. A Critical Evaluation of the Experimental and Theoretical Determination of Lithium Cation Affinities. *Int. J. Mass Spectrom.* **2007,** *267*, 167-182.
86. Woon, D. E.; Dunning, T. H., Jr. Gaussian basis sets for use in correlated molecular calculations. V. Core-valence basis sets for boron through neon. *J. Chem. Phys.* **1995,** *103*, 4572-4585.
87. Schuchardt, K. L.; Didier, B. T.; Elsethagen, T.; Sun, L.; Gurumoorthi, V.; Chase, J.; Li, J.; Windus, T. L. Basis Set Exchange: A Community Database for Computational Sciences. *J. Chem. Inf. Model.* **2007,** *47*, 1045-1052.
88. Feller, D. The Role of Databases in Support of Computational Chemistry Calculations. *J. Comput. Chem.* **1996,** *17*, 1571-1586.
89. Pritchard, B. P.; Altarawy, D.; Didier, B.; Gibson, T. D.; Windus, T. L. A New Basis Set Exchange: An Open, Up-to-date Resource for the Molecular Sciences Community. *J. Chem. Inf. Model.* **2019,** *59*, 4814-4820.
90. Rodgers, M. T.; Armentrout, P. B.; Oomens, J.; Steill, J. D. Infrared Multiphoton Dissociation Spectroscopy of Cationized Threonine: Effects of Alkali-Metal Cation Size on Gas-Phase Conformation. *J. Phys. Chem. A* **2008,** *112*, 2258-2267.
91. Citir, M.; Stennett, E. M. S.; Oomens, J.; Steill, J. D.; Rodgers, M. T.; Armentrout, P. B. Infrared Multiple Photon Dissociation Spectroscopy of Cationized Cysteine: Effects of Metal Cation Size on Gas-Phase Conformation. *Int. J. Mass Spectrom.* **2010,** *297*, 9-17.
92. Boles, G. C.; Coates, R. A.; Berden, G.; Oomens, J.; Armentrout, P. B. Experimental and Theoretical Investigations of Infrared Multiple Photon Dissociation Spectra of Glutamine Complexes with Zn^{2+} and Cd^{2+}. *J. Phys. Chem. B* **2015,** *119*, 11607–11617.
93. Boles, G. C.; Coates, R. A.; Berden, G.; Oomens, J.; Armentrout, P. B. Experimental and Theoretical Investigations of Infrared Multiple Photon Dissociation Spectra of Asparagine Complexes with Zn^{2+} and Cd^{2+} and Their Deamidation Processes. *J. Phys. Chem. B* **2016,** *120*, 12486-12500.
94. Boles, G. C.; Owen, C. J.; Berden, G.; Oomens, J.; Armentrout, P. B. Experimental and Theoretical Investigations of Infrared Multiple Photon Dissociation Spectra of Glutamic Acid Complexes with Zn^{2+} and Cd^{2+}. *Phys. Chem. Chem. Phys.* **2017,** *19*, 12394 - 12406.
95. Owen, C. J.; Boles, G. C.; Berden, G.; Oomens, J.; Armentrout, P. B. Experimental and Theoretical Investigations of Infrared Multiple Photon Dissociation Spectra of Lysine Complexes with Zn^{2+} and Cd^{2+}. *Eur. J. Mass Spectrom.* **2019,** *25*, 97-111.

96. Smith, S. M.; Markevitch, A. N.; Romanor, D. A.; Li, X.; Levis, R. J.; Schlegel, H. B. Static and Dynamic Polarizabilities of Conjugated Molecules and Their Cations *J. Phys. Chem. A* **2000,** *108*, 11063-11072.
97. Kebarle, P., Ion-Molecule Equilibria at High Pressure. In *Encyclopedia of Mass Spectrometry*, Armentrout, P. B., Ed. Elsevier: Amsterdam, 2003; Vol. 1, pp 319-338.
98. Gapeev, A.; Dunbar, R. C. Na^+ Affinities of Gas-phase Amino Acids by Ligand Exchange Equilibrium. *Int. J. Mass Spectrom.* **2003,** *228*, 825-839.
99. Wincel, H. Hydration Energies of Protonated Amino Acids. *Chem. Phys. Lett.* **2007,** *439*, 157-161.
100. Wincel, H. Hydration Energies of Sodiated Amino Acids from Gas-phase Equilibria Determinations. *J. Phys. Chem. A* **2007,** *111*, 5784–5791.
101. Wincel, H. Hydration of Potassiated Amino Acids in the Gas Phase. *J. Am. Soc. Mass Spectrom.* **2007,** *18*, 2083-2089.
102. Wincel, H. Hydration Energies of Deprotonated Amino Acids from Gas Phase Equilibria Measurements. *J. Am. Soc. Mass Spectrom.* **2008,** *19*, 1091-1097.
103. Dunbar, R. C.; McMahon, T. B.; Thoelmann, D.; Tonner, D. S.; Salahub, D. R.; Wei, D. Zero-Pressure Thermal-Radiation-Induced Dissociation of Gas-Phase Cluster Ions: Comparison of Theory and Experiment for $(H_2O)_2Cl^-$ and $(H_2O)_3Cl^-$. *J. Am. Chem. Soc.* **1995,** *117*, 12819–12825.
104. Price, W. D.; Schnier, P. D.; Williams, E. R. Tandem Mass Spectrometry of Large Biomolecule Ions by Blackbody Infrared Radiative Dissociation. *Anal. Chem.* **1996,** *68*, 859–866.
105. Dunbar, R. C. BIRD (blackbody infrared radiative dissociation): Evolution, principles, and applications. *Mass Spectrom. Rev.* **2004,** *23*, 127-158.
106. McLuckey, S. A.; Cameron, D.; Cooks, R. G. Proton Affinities from Dissociations of Proton-Bound Dimers. *J. Am. Chem. Soc.* **1981,** *103*, 1313-1317.
107. Cooks, R. G.; Wong, P. H. Kinetic Method of Making Thermochemical Determinations: Advances and Applications. *Acc. Chem. Res.* **1998,** *31*, 379-386.
108. Cheng, X.; Wu, Z.; Fenselau, C. Collision Energy Dependence of Proton-bound Dimer Dissociation: Entropy Effects, Proton Affinities, and Intramolecular Hydrogen-bonding in Protonated Peptides. *J. Am. Chem. Soc.* **1993,** *115*, 4844-4848.
109. Armentrout, P. B. Entropy Measurements and the Kinetic Method: A Statistically Meaningful Approach. *J. Am. Soc. Mass Spectrom.* **2000,** *11*, 371-379.
110. Armentrout, P. B. Is the Kinetic Method a Thermodynamic Method? *J. Mass Spectrom.* **1999,** *34*, 74-78.
111. Drahos, L.; Vekey, K. How Closely Related are the Effective and Real Temperature. *J. Mass Spectrom.* **1999,** *34*, 79-84.
112. Cooks, R. G.; Koskinen, J. T.; Thomas, P. D. The Kinetic Method of Making Thermochemical Determinations. *J. Mass Spectrom.* **1999,** *34*, 85-92.
113. Lee, S.; Wyttenbach, T.; Bowers, M. T. Gas phase structures of sodiated oligosaccharides by ion mobility/ion chromatography methods. *Int. J. Mass Spectrom.* **1997,** *167/168*, 605-614.
114. Hoaglund, C. S.; Valentine, S. J.; Clemmer, D. E. An Ion Trap Interface for ESI-Ion Mobility Experiments. *Anal. Chem.* **1997,** *69*, 4156-4161.

115. Kanu, A. B.; Dwivedi, P.; Tam, M.; Matz, L.; Hill, H. H. Ion Mobility-Mass Spectrometry. *J. Mass Spectrom.* **2008,** *43*, 1-22.
116. Moision, R. M.; Armentrout, P. B. An Experimental and Theoretical Dissection of Sodium Cation/Glycine Interactions. *J. Phys. Chem. A* **2002,** *106*, 10350-10362.
117. Moision, R. M.; Armentrout, P. B. An Experimental and Theoretical Dissection of Potassium Cation/Glycine Interactions. *Phys. Chem. Chem. Phys.* **2004,** *6*, 2588-2599.
118. Kapota, C.; Lemaire, J.; Maitre, P.; Ohanessian, G. Vibrational Signature of Charge Solvation vs Salt Bridge Isomers of Sodiated Amino Acids in the Gas Phase. *J. Am. Chem. Soc.* **2004,** *126*, 1836-1842.
119. Armentrout, P. B.; Stevenson, B. C.; Ghiassee, M.; Boles, G. C.; Berden, G.; Oomens, J. Infrared Multiple-photon Dissociation Spectroscopy of Cationized Glycine: Effects of Alkali Metal Cation Size on Gas-phase Conformation. *Phys. Chem. Chem. Phys.* **2022,** *24*, 22950-22959.
120. Jones, R. M.; Nilsson, T.; Walker, S.; Armentrout, P. B. Potassium Binding Interactions with Aliphatic Amino Acids: Thermodynamic and Entropic Effects Analyzed via a Guided Ion Beam and Computational Study. *J. Am. Soc. Mass Spectrom.* **2022,** *33*, 1427-1442.
121. Cohen, A. J.; Mori-Sánchez, P.; Yang, W. Challenges for Density Functional Theory. *Chem. Rev.* **2012,** *112*, 289-320.
122. Boese, A. D. Density Functional Theory and Hydrogen Bonds: Are We There Yet? *ChemPhysChem* **2015,** *16*, 978-985.
123. Rodgers, M. T.; Armentrout, P. B. Noncovalent Metal-Ligand Bond Energies as Studied by Threshold Collision-Induced Dissociation. *Mass Spectrom. Rev.* **2000,** *19*, 215-247.
124. Armentrout, P. B.; Rodgers, M. T. Thermochemistry of Non-Covalent Ion-Molecule Interactions. *Mass Spectrometry* **2013,** *2*, S0005.
125. Rodgers, M. T.; Armentrout, P. B. Cationic Noncovalent Interactions: Energetics and Periodic Trends. *Chem. Rev.* **2016,** *116*, 5642–5687
126. Jockusch, R. A.; Lemoff, A. S.; Williams, E. R. Hydration of Valine-Cation Complexes in the Gas Phase: On the Number of Water Molecules Necessary to Form a Zwitterion. *J. Phys. Chem. A* **2001,** *105*, 10929-10942.
127. Jockusch, R. A.; Lemoff, A. S.; Williams, E. R. Effect of Metal Ion and Water Coordination on the Structure of a Gas-phase Amino Acid. *J. Am. Chem. Soc.* **2001,** *123*, 12255–12265.
128. Lemoff, A. S.; Williams, E. R. Binding energies of water to lithiated valine: Formation of solution-phase structure in vacuo. *J. Am. Soc. Mass Spectrom.* **2004,** *15*, 1014-1024.
129. Armentrout, P. B.; Boles, G. C.; Ghiassee, M.; Berden, G.; Oomens, J. Infrared Multiple-Photon Dissociation Spectra of Sodiated Complexes of the Aliphatic Amino Acids. *J. Phys. Chem. A* **2021,** *125*, 6348-6355.
130. Pham, C. H.; Boles, G. C.; Armentrout, P. B. Sodium Binding Interactions with the Aliphatic Amino Acids: A Guided Ion Beam and Computational Study. *J. Phys. Chem. A* **2021,** *125*, 6332-6347.
131. Bojesen, G.; Breindahl, T.; Andersen, U. N. On the Sodium and Lithium Ion Affinities of Some α-Amino Acids. *Org. Mass Spectrom.* **1993,** *28*, 1448-1452.

132. Kish, M. M.; Ohanessian, G.; Wesdemiotis, C. The Na^+ Affinities of α-Amino Acids: Side-chain Substituent Effects. *Int. J. Mass Spectrom.* **2003,** *227*, 509-524.
133. Tsang, Y.; Wong, C. C. L.; Wong, C. H. S.; Cheng, J. M. K.; Ma, N. L.; Tsang, C. W. Proton and Potassium Affinities of Aliphatic and N-Methylated Aliphatic α-Amino Acids: Effect of Alkyl Chain Length on Relative Stabilities of K^+ Bound Zwitterionic Complexes. *Int. J. Mass Spectrom.* **2012,** *316-318*, 273-283.
134. Lemoff, A. S.; Bush, M. F.; Williams, E. R. Binding energies of water to sodiated valine and structural isomers in the gas phase: The effect of proton affinity on zwitterion stability. *J. Am. Chem. Soc.* **2003,** *125*, 13576–13584.
135. Kamariotis, A.; Boyarkin, O. V.; Mercier, S. R.; Beck, R. D.; Bush, M. F.; Williams, E. R.; Rizzo, T. R. Infrared Spectroscopy of Hydrated Amino Acids in the Gas Phase: Protonated and Lithiated Valine. *J. Am. Chem. Soc.* **2006,** *128*, 905-916.
136. Drayss, M. K.; Armentrout, P. B.; Oomens, J.; Schäfer, M. IR Spectroscopy of Cationized Aliphatic Amino Acids: Stability of Charge-solvated Structure Increases with Metal Cation Size. *Int. J. Mass Spectrom.* **2010,** *297*, 18–27.
137. Ye, S. J.; Moision, R. M.; Armentrout, P. B. Sequential Bond Energies of Water to Sodium Proline Cation. *Int. J. Mass Spectrom.* **2006,** *253*, 288-304.
138. Drayss, M. K.; Blunk, D.; Oomens, J.; Schäfer, M. Infrared Multiple Photon Dissociation Spectroscopy of Potassiated Proline. *J. Phys Chem. A* **2008,** *112*, 11972-11974.
139. Carl, D. R.; Cooper, T. E.; Oomens, J.; Steill, J. D.; Armentrout, P. B. Infrared Multiple Photon Dissociation Spectroscopy of Cationized Methionine: Effects of Alkali-Metal Cation Size on Gas-Phase Conformation. *Phys. Chem. Chem. Phys.* **2010,** *12*, 3384-3398.
140. Dunbar, R. C.; Steill, J. D.; Oomens, J. Cationized phenylalanine conformations characterized by IRMPD and computation for singly and doubly charged ions. *Phys. Chem. Chem. Phys.* **2010,** *12*, 13383-13393.
141. Polfer, N. C.; Paizs, B.; Snoek, L. C.; Compagnon, I.; Suhai, S.; Meijer, G.; von Helden, G.; Oomens, J. Infrared Fingerprint Spectroscopy and Theoretical Studies of Potassium Ion Tagged Amino Acids and Peptides in the Gas Phase. *J. Am. Chem. Soc.* **2005,** *127*, 8571-8579.
142. Ruan, C.; Rodgers, M. T. Cation-π Interactions: Structures and Energetics of Complexation of Na^+ and K^+ with the Aromatic Amino Acids, Phenylalanine, Tyrosine and Tryptophan. *J. Am. Chem. Soc.* **2004,** *126*, 14600-14610.
143. Armentrout, P. B.; Yang, B.; Rodgers, M. T. Metal Cation Dependence of Interactions with Amino Acids: Bond Energies of Rb^+ and Cs^+ to Met, Phe, Tyr, and Trp. *J. Phys. Chem. B* **2013,** *117*, 3771-3781.
144. Polfer, N. C.; Oomens, J.; Dunbar, R. C. IRMPD Spectroscopy of Metal-Ion/Tryptophan Complexes. *Phys. Chem. Chem. Phys.* **2006,** *8*, 2744-2751.
145. O'Brien, J. T.; Prell, J. S.; Steill, J. D.; Oomens, J.; Williams, E. R. Interactions of Mono- and Divalent Metal Ions with Aspartic and Glutamic Acid Investigated with IR Photodissociation Spectroscopy and Theory. *J. Phys. Chem. A* **2008,** *112*, 10823-10830.
146. Armentrout, P. B.; Yang, B.; Rodgers, M. T. Metal Cation Dependence of Interactions with Amino Acids: Bond Dissociation Energies of Rb^+ and Cs^+ to the Acidic Amino Acids and Their Amide Derivatives. *J. Phys. Chem. B* **2014,** *118*, 4300–4314.

147. Heaton, A. L.; Bowman, V. N.; Oomens, J.; Steill, J. D.; Armentrout, P. B. Infrared Multiple Photon Dissociation Spectroscopy of Cationized Asparagine: Effects of Metal Cation Size on Gas-Phase Conformation. *J. Phys. Chem. A* **2009,** *113*, 5519-5530.
148. Bush, M. F.; Oomens, J.; Saykally, R. J.; Williams, E. R. Alkali Metal Ion Binding to Glutamine and Glutamine Derivatives Investigated by Infrared Action Spectroscopy and Theory. *J. Phys. Chem. A* **2008,** *112*, 8578-8584.
149. Bush, M. F.; Forbes, M. W.; Jockusch, R. A.; Oomens, J.; Polfer, N. C.; Saykally, R. J.; Williams, E. R. Infrared Spectroscopy of Cationized Lysine and ε-N-methyllysine in the Gas Phase: Effects of Alkali-Metal Ion Size and Proton Affinity on Zwitterion Stability. *J. Phys. Chem. A* **2007,** *111*, 7753-7760.
150. Clark, A. A.; Yang, B.; Rodgers, M. T.; Armentrout, P. B. Experimental and Computational Study of the Group 1 Metal Cation Chelates with Lysine: Bond Dissociation Energies, Structures, and Structural Trends. *J. Phys. Chem. B* **2019,** *123*, 1983-1997.
151. Bush, M. F.; O'Brien, J. T.; Prell, J. S.; Saykally, R. J.; Williams, E. R. Infrared Spectroscopy of Cationized Arginine in the Gas Phase: Direct Evidence for the Transition from Nonzwitterionic to Zwitterionic Structure. *J. Am. Chem. Soc.* **2007,** *129*, 1612-1622.
152. Forbes, M. W.; Bush, M. F.; Polfer, N. C.; Oomens, J.; Dunbar, R. C.; Williams, E. R.; Jockusch, R. A. Infrared Spectroscopy of Arginine Cation Complexes: Direct Observation of Gas-Phase Zwitterions. *J. Phys. Chem. A* **2007,** *111*, 11759-11770.
153. Citir, M.; Hinton, C. S.; Oomens, J.; Steill, J. D.; Armentrout, P. B. Infrared Multiple Photon Dissociation Spectroscopy of Cationized Histidine: Effects of Metal Cation Size on Gas-Phase Conformation. *J. Phys. Chem. A* **2012,** *116*, 1532-1541.
154. Dunbar, R. C.; Hopkinson, A. C.; Oomens, J.; Siu, C.-K.; Siu, K. W. M.; Steill, J. D.; Verkerk, U. H.; Zhao, J. Conformation Switching in Gas-Phase Complexes of Histidine with Alkaline Earth Ions. *J. Phys. Chem. B* **2009,** *113*, 10403-10408.
155. Bush, M. F.; Oomens, J.; Williams, E. R. Proton Affinity and Zwitterion Stability: New Results from Infrared Spectroscopy and Theory of Cationized Lysine and Analogues in the Gas Phase. *J. Phys. Chem. A* **2009,** *113*, 431-438.
156. Polfer, N. C.; Dunbar, R. C.; Oomens, J. Observation of Zwitterion Formation in the Gas-Phase H/D-Exchange with CH_3OD: Solution-Phase Structures in the Gas Phase. *J. Am. Soc. Mass Spectrom.* **2007,** *18*, 512-516.
157. Ye, S. J.; Armentrout, P. B. Guided Ion Beam and Theoretical Studies of Sequential Bond Energies of Water to Sodium Cysteine Cation. *Phys. Chem. Chem. Phys.* **2010,** *12*, 13419-13433.
158. Steinhardt, J.; Reynolds, J. A., *Multiple equilibria in proteins*. Academic Press: New York, 1969.
159. Lemoff, A. S.; Bush, M. F.; Wu, C.-C.; Williams, E. R. Structures and hydration enthalpies of cationized glutamine and structural analogues in the gas phase. *J. Am. Chem. Soc.* **2005,** *127*, 10276-10286.
160. Lemoff, A. S.; Wu, C.-C.; Bush, M. F.; Williams, E. R. Binding energies of water to doubly hydrated cationized glutamine and structural analogues in the gas phase. *J. Phys. Chem. A* **2006,** *110*, 3662-3669.
161. Lemoff, A. S.; Bush, M. F.; O'Brien, J. T.; Williams, E. R. Structures of Lithiated Lysine and Structural Analogues in the Gas Phase: Effects of Water and Proton Affinity on Zwitterionic Stability *J. Phys. Chem. A* **2006,** *110*, 8433-8442.

162. Armentrout, P. B.; Armentrout, E. I.; Clark, A. A.; Cooper, T. E.; Stennett, E. M. S.; Carl, D. R. An Experimental and Theoretical Study of Alkali Metal Cation Interactions with Cysteine. *J. Phys. Chem. B* **2010,** *114*, 3927-3937.
163. Armentrout, P. B.; Citir, M.; Chen, Y.; Rodgers, M. T. Thermochemistry of Alkali Metal Cation Interactions with Histidine: Influence of the Side-Chain. *J. Phys. Chem. A* **2012,** *116*, 11823-11832.
164. Bowman, V. N.; Heaton, A. L.; Armentrout, P. B. Metal Cation Dependence of Interactions with Amino Acids: Bond Energies of Rb^+ to Gly, Ser, Thr, and Pro. *J. Phys. Chem. B* **2010,** *114*, 4107-4114.
165. Armentrout, P. B.; Gabriel, A.; Moision, R. M. An Experimental and Theoretical Study of Alkali Metal Cation/Methionine Interactions. *Int. J. Mass Spectrom.* **2009,** *283*, 56-68.
166. Mookherjee, A.; Armentrout, P. B. Theoretical Investigation and Reinterpretation of the Decomposition of Lithiated Proline and N-Methyl Proline. *Int. J. Mass Spectrom.* **2014,** *370*, 16-28.
167. Mookherjee, A.; Armentrout, P. B. Role of Methylation on the Thermochemistry of Alkali Metal Cation Complexes of Amino Acids: N-Methyl Proline. *Int. J. Mass Spectrom.* **2013,** *345-347*, 109-119.
168. Ye, S. J.; Clark, A. A.; Armentrout, P. B. An Experimental and Theoretical Investigation of Alkali Metal Cation Interactions with Hydroxyl Side Chain Amino Acids. *J. Phys. Chem. B* **2008,** *112*, 10291-10302.
169. Wang, P.; Ohanessian, G.; Wesdemiotis, C. The Sodium Ion Affinities of Asparagine, Glutamine, Histidine and Arginine. *Int. J. Mass Spectrom.* **2008,** *269*, 34-45.
170. Wilson, R. G.; Brewer, G. R., *Ion Beams with Applications to Ion Implantation*. Wiley: New York, 1973.
171. Rodgers, M. T.; Armentrout, P. B., Discriminating Properties of Metal Alkali Ions towards the Constituents of Proteins and Nucleic Acids. Conclusions from Gas-Phase and Theoretical Studies. In *Metal Ions in Life Sciences. Volume 16: The Alkali Metal Ions: Their Role for Life*, Sigel, A.; Sigel, H.; Sigel, R. K. O., Eds. Springer: Cham, Switzerland, 2016; pp 103-131.
172. Lide, D. R., *CRC Handbook of Chemistry and Physics*. CRC Press: Boca Raton, 2002; Vol. 83.
173. Balaj, O. P.; Kapota, C.; Lemaire, J.; Ohanessian, G. Vibrational signatures of sodiated oligopeptides (GG-Na^+, GGG-Na^+, AA-Na^+ and AAA-Na^+) in the gas phase. *Int. J. Mass Spectrom.* **2008,** *269*, 196-209.
174. Klassen, J. S.; Anderson, S. G.; Blades, A. T.; Kebarle, P. Reaction Enthalpies for $M^+L = M^+ + L$, Where $M^+ = Na^+$ and K^+ and L = Acetamide, N-methylacetamide, N,N-dimethylacetamide, Glycine, and Glycylglycine, from Determinations of the Collision-induced Dissociation Thresholds. *J. Phys. Chem.* **1996,** *100*, 14218-14227.
175. Wang, P.; Wesdemiotis, C.; Kapota, C.; Ohanessian, G. The Sodium Ion Affinities of Simple Di-, Tri-, and Tetrapeptide. *J. Am. Soc. Mass Spectrom.* **2007,** *18*, 541-552.
176. Dunbar, R. C.; Steill, J. D.; Oomens, J. Conformations and Vibrational Spectroscopy of Metal Ion/Polylalanine Complexes. *Int. J. Mass Spectrom.* **2010,** *297*, 107-115.
177. Dunbar, R. C.; Steill, J.; Polfer, N. C.; Oomens, J. Peptide Length, Steric Effects and Ion Solvation Govern Zwitterion Stabilization in Barium-Chelated Di- and Tripeptides. *J. Phys. Chem. B* **2009,** *113*, 10552-10554.

178. Dunbar, R. C.; Polfer, N. C.; Berden, G.; Oomens, J. Metal ion binding to peptides: Oxygen or nitrogen sites? *Int. J. Mass Spectrom.* **2012,** *330-332*, 71-77.
179. Benzakour, M.; Mcharfi, M.; Cartier, A.; Daoudi, A. Interactions of Peptides with Metallic Cations. I. Complexes Glycylglycine–M^+ (M = Li, Na). *J. Mol. Struct. Theochem.* **2004,** *710*, 169-174.
180. Cerda, B. A.; Hoyau, S.; Ohanessian, G.; Wesdemiotis, C. Na^+ Binding to Cyclic and Linear Dipeptides. Binding Energies, Entropies of Na^+ Complexation, and Attachment Sites from the Dissociation of Na^+-bound Heterodimers and Ab Initio Calculations. *J. Am. Chem. Soc.* **1998,** *120*, 2437-2448.
181. Kish, M. M.; Wesdemiotis, C.; Ohanessian, G. The Sodium Ion Affinity of Glycylglycine. *J. Phys. Chem. B* **2004,** *108*, 3086-3091.
182. Wong, C. H. S.; Ma, N. L.; Tsang, C. W. A Theoretical Study of Potassium Cation Binding to Glycylglycine (GG) and Alanylalanine (AA) Dipeptides. *Chem. Eur. J.* **2002,** *8*, 4909-4918.
183. Polfer, N. C.; Oomens, J.; Dunbar, R. C. Alkali metal complexes of the Dipeptides PheAla and AlaPhe : IRMPD spectroscopy. *ChemPhysChem* **2008,** *9*, 579-589.
184. Dunbar, R. C.; Oomens, J.; Berden, G.; Lau, J. K.-C.; Verkerk, U. H.; Hopkinson, A. C.; Siu, K. W. M. Metal Ion Complexes with HisGly: Comparison with PhePhe and PheGly. *J. Phys. Chem. A* **2013,** *117*, 5335-5343.
185. Dunbar, R. C.; Steill, J. D.; Oomens, J. Encapsulation of Metal Cations by the PhePhe Ligand: A Cation-π Ion Cage. *J. Am. Chem. Soc.* **2011,** *133*, 9376-9386.
186. Prell, J. S.; Demireva, M.; Oomens, J.; Williams, E. R. Role of Sequence in Salt-Bridge Formation for Alkali Metal Cationized GlyArg and ArgGly Investigated with IRMPD Spectroscopy and Theory. *J. Am. Chem. Soc.* **2009,** *131*, 1232-1242.
187. Prell, J. S.; Chang, T. M.; Biles, J. A.; Berden, G.; Oomens, J.; Williams, E. R. Isomer Population Analysis of Gaseous Ions From Infrared Multiple Photon Dissociation Kinetics. *J. Phys. Chem. A* **2011,** *115*, 2745-2751.
188. Balaj, O. P.; Semrouni, D.; Steinmetz, V.; Nicol, E.; Clavaguera, C.; Ohanessian, G. Structure of Sodiated Polyglycines. *Chem.-Eur. J.* **2012,** *18*, 4583-4592.
189. Semrouni, D.; Balaj, O. P.; Calvo, F.; Correia, C. F.; Clavaguéra, C.; Ohanessian, G. Structure of Sodiated Octa-Glycine: IRMPD Spectroscopy and Molecular Modeling. *J. Am. Soc. Mass Spectrom.* **2010,** *21*, 728-738.
190. Dunbar, R. C.; Steill, J. D.; Polfer, N. C.; Oomens, J. Metal Cation Binding to Gas-Phase Pentaalanine: Divalent Ions Restructure the Complex. *J. Phys. Chem. A* **2012,** *117*, 1094-1101.
191. Martens, J. K.; Compagnon, I.; Nicol, E.; McMahon, T. B.; Clavaguera, C.; Ohanessian, G. Globule to Helix Transition in Sodiated Polyalanines. *J. Phys. Chem. Lett.* **2012,** *3*, 3320-3324.
192. Kohtani, M.; Kinnear, B. S.; Jarrold, M. F. Metal-Ion Enhanced Helicity in the Gas Phase. *J. Am. Chem. Soc.* **2000,** *122*, 12377-12378.
193. Kohtani, M.; Jarrold, M. F.; Wee, S.; O'Hair, R. A. J. Metal Ion Interactions with Polyalanine Peptides. *J. Phys. Chem. B* **2004,** *108*, 6093-6097.
194. Rogalewicz, F.; Hoppilliard, Y.; Ohanessian, G. Structures and fragmentations of zinc(II) complexes of amino acids in the gas phase. I. Electrosprayed ions which are

structurally different from their liquid phase precursors. *Int. J. Mass Spectrom.* **2000,** *201*, 307-320.
195. Hoppilliard, Y.; Rogalewicz, F.; Ohanessian, G. Structures and fragmentations of zinc(II) complexes of amino acids in the gas phase. II. Decompositions of glycine–Zn(II) complexes. *Int. J. Mass Spectrom.* **2001,** *204*, 267-280.
196. Rogalewicz, F.; Hoppilliard, Y.; Ohanessian, G. Structures and fragmentations of zinc(II) complexes of amino acids in the gas phase. III. Rearrangement versus desolvation in the electrospray formation of the glycine-zinc complex. *Int. J. Mass Spectrom.* **2001,** *206*, 45-52.
197. Rogalewicz, F.; Hoppilliard, Y.; Ohanessian, G. Structures and fragmentations of zinc(II) complexes of amino acids in the gas phase: IV. Solvent effect on the structure of electrosprayed ions. *Int. J. Mass Spectrom.* **2003,** *227*, 439-451.
198. Polfer, N. C.; Oomens, J.; Moore, D. T.; von Helden, G.; Meijer, G.; Dunbar, R. C. Infrared Spectroscopy of Phenylalanine Ag(I) and Zn(II) Complexes in the Gas Phase. *J. Am. Chem. Soc.* **2006,** *128*, 517-525.
199. Dunbar, R. C.; Polfer, N. C.; Oomens, J. Gas-phase zwitterion stabilization by a metal dication. *J. Am. Chem. Soc.* **2007,** *129*, 14562-14563.
200. Dunbar, R. C.; Steill, J. D.; Polfer, N. C.; Oomens, J. Dimeric Complexes of Tryptophan with M^{2+} Metal Ions. *J. Phys. Chem. A* **2009,** *113*, 845-851.
201. Atkins, C. G.; Banu, L.; Rowsell, M.; Blagojevic, V.; Bohme, D. K.; Fridgen, T. D. Structure of [Pb(Gly-H)]+ and the Monosolvated Water and Methanol Solvated Species by Infrared Multiple-Photon Dissociation Spectroscopy, Energy-Resolved Collision-Induced Dissociation, and Electronic Structure Calculations. *J. Phys. Chem. B* **2009,** *113*, 14457-14464.
202. Burt, M. B.; Decker, S. G. A.; Atkins, C. G.; Rowsell, M.; Peremans, A.; Fridgen, T. D. Structures of Bare and Hydrated [Pb(AminoAcid-H)]+ Complexes Using Infrared Multiple Photon Dissociation Spectroscopy. *J. Phys. Chem. B* **2011,** *115*, 11506-11518.
203. Banu, L.; Blagojevic, V.; Bohme, D. Dissociation of deprotonated glycine complexes with Pb2+ and five transition-metal dications (Fe2+, Co2+, Ni2+, Cu2+, Zn2+): The importance of metal bond activation. *Int. J. Mass Spectrom.* **2012,** *330-332*, 168-173.
204. Banu, L.; Blagojevic, V.; Bohme, D. Bond activation in complexes of Pb(II) with 15 deprotonated amino acids: Correlation with gas-phase acidity. *Int. J. Mass Spectrom.* **2012,** *316*, 23-30.
205. Gholami, A.; Fridgen, T. D. Structures and Unimolecular Reactivity of Gas-Phase $[Zn(Proline-H)]^+$ and $[Zn(Proline-H)(H_2O)]^+$. *J. Phys. Chem. B* **2013,** *117*, 8447-8456.
206. Burt, M. B.; Fridgen, T. D. Gas-Phase Structures of Pb2+-Cationized Phenylalanine and Glutamic Acid Determined by Infrared Multiple Photon Dissociation Spectroscopy and Computational Chemistry. *J. Phys. Chem. A* **2013,** *117*, 1283-1290.
207. Dunbar, R. C.; Berden, G.; Martens, J. K.; Oomens, J. Divalent Metal-Ion Complexes with Dipeptide Ligands Having Phe and His Side-Chain Anchors: Effects of Sequence, Metal Ion, and Anchor. *J. Phys. Chem. A* **2015,** *119*, 9901-9909.
208. Dunbar, R. C.; Martens, J.; Berden, G.; Oomens, J. Complexes of Ni(ii) and Cu(ii) with small peptides: deciding whether to deprotonate. *Phys. Chem. Chem. Phys.* **2016,** *18*, 26923-26932.

209. Dunbar, R. C.; Martens, J.; Berden, G.; Oomens, J. Transition Metal(II) Complexes of Histidine-containing Tripeptides: Structures, and Infrared Spectroscopy by IRMPD. *Int. J Mass Spectrom.* **2018,** *429*, 198-205.
210. Peckelsen, K.; Martens, J.; Berden, G.; Oomens, J.; Dunbar, R. C.; Meijer, A. J. H. M.; Schäfer, M. Gas-phase Complexes of Ni^{2+} and Ca^{2+} with Deprotonated Histidylhistidine (HisHis): A Model Case for Polyhistidyl-metal Binding Motifs. *J. Mol. Spec.* **2017,** *332*, 38-44.
211. Hofstetter, T. E.; Howder, C.; Berden, G.; Oomens, J.; Armentrout, P. B. Structural Elucidation of Biological and Toxicological Complexes: Investigation of Monomeric and Dimeric Complexes of Histidine with Multiply Charged Transition Metal (Zn and Cd) Cations using IR Action Spectroscopy. *J. Phys. Chem. B* **2011,** *115*, 12648-12661.
212. Coates, R. A.; McNary, C. P.; Boles, G. C.; Berden, G.; Oomens, J.; Armentrout, P. B. Structural Characterization of Gas-Phase Cysteine and Cysteine Methyl Ester Complexes with Zinc and Cadmium Dications by Infrared Multiple Photon Dissociation Spectroscopy. *Phys. Chem. Chem. Phys.* **2015,** *17*, 25799-25808.
213. Coates, R. A.; Boles, G. C.; McNary, C. P.; Berden, G.; Oomens, J.; Armentrout, P. B. Zn^{2+} and Cd^{2+} Cationized Serine Complexes: Infrared Multiple Photon Dissociation Spectroscopy and Density Functional Theory Investigations. *Phys. Chem. Chem. Phys.* **2016,** *18*, 22434 – 22445.
214. Boles, G. C.; Hightower, R. L.; Coates, R. A.; McNary, C. P.; Berden, G.; Oomens, J.; Armentrout, P. B. Experimental and Theoretical Investigations of Infrared Multiple Photon Dissociation Spectra of Aspartic Acid Complexes with Zn^{2+} and Cd^{2+}. *J. Phys. Chem. B* **2018,** *122*, 3836-3853.
215. Chalifoux, A. M.; Boles, G. C.; Berden, G.; Oomens, J.; Armentrout, P. B. Experimental and Theoretical Investigations of Infrared Multiple Photon Dissociation Spectra of Arginine Complexes with Zn^{2+} and Cd^{2+}. *Phys. Chem. Chem. Phys.* **2018,** *20*, 20712-20725.
216. Boles, G. C.; Hightower, R. L.; Berden, G.; Oomens, J.; Armentrout, P. B. Zinc and Cadmium Complexation of l-Threonine: An Infrared Multiple Photon Dissociation Spectroscopy and Theoretical Study. *J. Phys. Chem. B* **2019,** *123*, 9343-9354.
217. Stevenson, B. C.; Martens, J.; Berden, G.; Oomens, J.; Schäfer, M.; Armentrout, P. B. IRMPD Spectroscopic and Theoretical Structural Investigations of Zinc and Cadmium Dications Bound to Histidine Dimers. *J. Phys. Chem. A* **2020,** *124*, 10266-10276.
218. Boles, G. C.; Stevenson, B. C.; Hightower, R. L.; Berden, G.; Oomens, J.; Armentrout, P. B. Zinc and cadmium complexation of L-methionine: An infrared multiple photon dissociation spectroscopy and theoretical study. *J. Mass Spectrom.* **2021,** *56*, e4580.
219. Stevenson, B. C.; Martens, J.; Berden, G.; Oomens, J.; Armentrout, P. B. Spectroscopic Investigation of the Metal Coordination of the Aromatic Amino Acids with Zinc and Cadmium. *J. Phys. Chem. A* **2023,** *127*, 3560-3569.
220. Stevenson, B. C.; Berden, G.; Martens, J.; Oomens, J.; Armentrout, P. B. Determining gas-phase chelation of zinc, cadmium, and copper cations with HisHis dipeptide using action spectroscopy and theoretical calculations. *Int. J. Mass Spectrom.* **2024,** *495*, 117154.
221. Pavletich, N. P.; Pabo, C. O. Zinc Finger-DNA Recognition: Crystal Structure of a Zif268-DNA Complex at 2.1 Å. *Science* **1991**, 809-817.

222. Fairall, L.; Schwabe, J. W. R.; Chapman, L.; Finch, J. T.; Rhodes, D. The Crystal Structure of a Two Zinc-finger Peptide Reveals an Extension to the Rules for Zinc-finger/DNA Recognition. *Nature* **1993,** *366*, 483 - 487.
223. Berg, J. M.; Shi, Y., The Galvanization of Biology: A Growing Appreciation for the Roles of Zinc. In *Science*, 1996; Vol. 271, pp 1081-1085.
224. Mackay, J. P.; Crossley, M. Zinc Fingers are Sticking Together. *Trends Biochem. Sci.* **1998,** *23*, 1-4.
225. Iuchi, S.; Kuldell, N., *Zinc Finger Proteins From Atomic Contact to Cellular Function*. Kluwer Academic/Plenum New York, 2005.
226. Spiro, T. G., *Zinc enzymes*. J. Wiley: New York, 1983.
227. Hartwig, A.; Asmuss, M.; Blessing, H.; Hoffmann, S.; Jahnke, G.; Khandelwal, S.; Pelzer, A.; Burkle, A. Interference by Toxic Metal Ions with Zinc-dependent Proteins Involved in Maintaining Genomic Stability. *Food Chem. Toxicol.* **2002,** *40*, 1179-1184.
228. Asmuss, M.; Mullenders, L. H. F.; Eker, A.; Hartwig, A. Differential Effects of Toxic Metal Compounds on the Activities of Fpg and XPA, Two Zinc Finger Proteins Involved in DNA Repair. *Carcinogenesis* **2000,** *21*, 2097-2104.
229. Price, N. M.; Morel, F. M. M. Cadmium and Cobalt Substitution for Zinc in a Marine Diatom. *Nature* **1990,** *344*, 658-660.
230. Walker, S. K.; Stevenson, B. C.; III, R. M. J.; Berden, G.; Martens, J.; Oomens, J.; Armentrout, P. B. Structural characterizations of histidine-containing tripeptides complexed with zinc and cadmium dications in the gas-phase using IRMPD and theoretical calculations. work in progress.

Table 1. Structures of M^+(Xxx) complexes of alkali metal cations with amino acids determined primarily by IR spectroscopy.[a]

Xxx	Li^+	Na^+	K^+	Rb^+	Cs^+
Gly	[N,CO] [b]	[N,CO] [b,c]	[CO,OH], [CO] [b]	[CO], [CO,OH] [b]	[CO,OH] [d]
Pro [e]	[CO_2^-]	[CO_2^-][c]	[CO_2^-], [CO,OH][f]	[CO_2^-], [CO,OH]	[CO,OH], [CO_2^-]
Ser [g]	[N,CO,SC]	[N,CO,SC]	[N,CO,SC], [CO,OH]	[N,CO,SC], [CO,OH]	[N,CO,SC], [CO,OH], [CO_2^-]
Thr [h]	[N,CO,SC]	[N,CO,SC]	[N,CO,SC], [CO,OH]	[N,CO,SC], [CO,OH]	[N,CO,SC], [CO,OH], [CO_2^-]
Cys [i]	[N,CO,SC]	[N,CO,SC]	[CO,OH], [N,CO,SC], [CO_2^-]	[CO,OH], [N,CO,SC], [CO_2^-]	[CO,OH], [N,CO,SC], [CO_2^-]
Met [j]	[N,CO,SC]	[N,CO,SC]	[N,CO,SC], [CO_2^-], [CO,OH,SC]?	[N,CO,SC], [CO_2^-], [CO,OH,SC]?	[N,CO,SC], [CO_2^-], [CO,OH,SC]?
Phe [k]	[N,CO,SC]	[N,CO,SC]	[N,CO,SC] [l]	[N,CO,SC], [CO,SC]	[N,CO,SC], [CO,OH], [CO,SC]
Tyr [l]		*[N,CO,SC]* [m]	[N,CO,SC]	*[N,CO,SC], [CO,SC]* [n]	*[N,CO,SC], [CO,SC]*[n]
Trp [o]	[N,CO,SC]	[N,CO,SC], [CO,SC]	[N,CO,SC], [CO,SC]	[CO,SC], [N,CO,SC]	[CO,SC], [N,CO,SC]
Asp [p]	[N,CO,SC]	*[N,CO,SC]* [q]	*[N,CO,SC]* [r]	*[N,CO,SC]* [s]	[CO,OH,SC], [N,CO,SC][s]
Glu [p]	[N,CO,SC]	*[N,CO,SC]* [q]	*[N,CO,SC], [CO_2^-]* [r]	*[N,CO,SC], [CO,OH,SC]* [s]	[CO,OH,SC], [CO,SC], [N,CO,SC][s]
Asn [t]	[N,CO,SC]	[N,CO,SC]	[N,CO,SC], [CO,OH,SC]	[N,CO,SC], [CO,OH,SC]	[N,CO,SC], [CO,OH,SC]

Gln [u]	[N,CO,SC]	[N,CO,SC], [CO,SC], [CO,OH,SC]?	[N,CO,SC], [CO,SC], [CO,OH,SC]?	*[CO,OH,SC]* [s]	[CO,OH,SC], [CO,SC], [N,CO,SC]
Lys [v]	[N,CO,SC]	[N,CO,SC]	[CO,OH,SC], [CO_2^-,SC] [w]	*[CO,OH,SC]* [w]	[CO,OH,SC], [CO_2^-,SC] [w]
Arg [x]	[N,CO,SC]	[CO_2^-], [N,CO,SC]	[CO_2^-]	[CO_2^-]	[CO_2^-]
His [y]	[N,CO,SC]	[N,CO,SC] [z]	[CO,SC], [N,CO,SC], [CO,OH]	[CO,SC], [N,CO,SC], [CO,OH]	[CO,SC], [CO,OH], [N,CO,SC]

[a] Isomers are given in order of approximate relative population, ? = may be present. SC = side-chain heteroatom or aromatic ring. Entries in italics are global minimum structures from computational studies. [b] Ref. *119*. [c] Ref. 118. [d] Ref. 80. [e] Ref. 136. [f] Ref. 138. [g] Ref. 64. [h] Ref. 90. [i] Ref. 91. [j] Ref. 139. [k] Ref. 140. [l] Ref. 141. [m] Ref. 142. [n] Ref. *143*. [o] Ref. 144. [p] Ref. 145. [q] Ref. 29. [r] Ref. *47*. [s] Ref. *146*. [t] Ref. 147. [u] Ref. 148. [v] Ref. 149. [w] Ref. *150*. [x] Ref. 151, 152. [y] Ref. 153. [z] Ref. 154.

Table 2. Bond dissociation energies (kJ/mol) at 0 K of M^+(Xxx) complexes of alkali metal cations with amino acids and small peptides and their polarizabilities (α).[a]

Xxx	α (Å^3)	Li^+	Na^+	K^+	Rb^+	Cs^+
Gly	6.6	220.0 (8.0)[b]	164.0 (4.8)[c]	118.3 (4.2)[d,e]	108.7 (7.0)[f]	93.3 (2.5)[g]
Ala	8.2		167.1 (7.3) [h]	120.6 (3.9) [e]		
hAla	10.1		168.1 (7.4) [h]	125.2 (4.9) [e]		
Val	12.0		172.4 (8.2) [h]	124.5 (4.4) [e]		
Leu	13.9		174.1 (6.9) [h]	127.4 (5.8) [e]		
Ile	14.0		174.3 (7.0) [h]	126.7 (5.2) [e]		
Cys	11.2	255.8 (11.9)[i]	176.9 (5.0)[i]	120.7 (3.1)[i]	102.5 (2.8)[i]	96.8 (4.2)[g]
Pro	10.8	254.7 (6.8)[j]	186.2 (4.8)[k]	143.5 (4.5)[k]	125.2 (4.5)[f]	107.9 (4.6)[g]
Asp	10.4		194.9 (5.8)[l]	147.6 (6.8)[m]	126.1 (6.8)[n]	108.9 (6.7)[n]
Glu	12.2		198.8 (4.8)[l]	152.4 (6.8)[m]	134.2 (7.7)[n]	112.6 (6.5)[n]
Ser	8.6	280.8 (12.5)[o]	199.7 (7.7)[o]	144.7 (6.8)[o]	115.7 (4.9)[f]	102.3 (4.1)[g]
Met	14.6	292.0 (12.2)[p]	201.7 (10.6)[p]	141.8 (10.6)[p]	121.0 (7.0)[q]	102.8 (6.6)[q]
Thr	10.5	284.6 (13.5)[o]	203.6 (9.6)[o]	148.6 (9.6)[o]	122.1 (4.6)[f]	105.4 (4.3)[g]
Phe	18.1		205.5 (6.8)[r]	150.5 (5.8)[r]	123.8 (7.2)[q]	112.9 (5.5)[q]
Tyr	18.8		209.4 (9.6)[r]	155.3 (8.7)[r]	125.8 (7.4)[q]	115.6 (6.9)[q]
Asn	11.2		209.4 (5.8)[l]	156.3 (6.8)[m]	138.4 (7.1)[n]	115.3 (6.9)[n]
Gln	13.0		213.2 (5.8)[l]	161.1 (7.7)[m]	144.2 (9.2)[n]	128.1 (8.5)[n]
Trp	22.0		217.1 (7.7)[r]	165.0 (5.8)[r]	138.1 (7.5)[q]	125.0 (6.8)[q]
Lys	14.5	<376 (30)[s]	219 (13)[s]	160 (10)[s]	141 (6)[s]	128 (4)[s]
His	15.2		222.5 (11.0)[t]	163.5 (8.5)[t]	137.4 (5.7)[t]	118.2 (6.4)[t]
Arg			*242 (8)*[u]			
GG	11.3		209 (13)[v]	149 (7)[v]		
GGG	16.2		240 (17)[v]	183 (15)[v]		
GGGG	21.1		*261 (11)*[w]			

[a] Uncertainties in parentheses. All values obtained by TCID except as noted. [b] Ref. 85. [c] Ref. 116. [d] Ref. 117. [e] Ref. 120. [f] Ref. 164. [g] Ref. 25. [h] Ref. 130. [i] Ref. 162. [j] Ref. 166. [k] Ref. 67. [l] Ref. 29. [m] Ref. 47. [n] Ref. 146. [o] Ref. 168. [p] Ref. 165. [q] Ref. 143. [r] Ref. 142. [s] Ref. 150. [t] Ref. 163. [u] Ref. 169 (*kinetic method*). [v] Ref. 27. [w] Ref. 175 (*kinetic method*).

Table 3. Structures of M^+(Xxx) complexes of group 12 dications with amino acids.[a]

Xxx	$Zn(Xxx-H)^+$	$ZnCl^+(Xxx)$	$Cd^+(Xxx-H)^+$	$CdCl^+(Xxx)$
Gly [b,c]	[N,CO^-]			
Ser [d]	[N,CO,SC^-]			[N,CO,SC]
Thr [b]	[N,CO^-,SC],			[N,CO,SC]
	[N,CO,SC^-]			
Cys [e]	[N,CO,SC^-]		[N,CO,SC^-]	
CysOMe [e]	[N,CO,SC^-]		[N,CO,SC^-]	[N,CO,SC]
Met [f]	[N,CO^-,SC]	[N,CO,SC]		[N,CO,SC]
Phe [g]		[N,CO,SC]		[N,CO,SC]
Tyr [g]		[N,CO,SC]		[N,CO,SC]
Trp [g,h200, 219]		[N,CO,SC]		[N,CO,SC]
Asp [i]	[N,CO^-,SC](L)			[N,CO,SC]
Asp-NH_3 [i]	[CO_2^-,SC]			
Glu [j]	[N,CO^-,SC]			[N,CO,SC]
Asn [k]	[N,CO^-,SC]			[N,CO,SC]
Asn-NH_3 [i]	[CO_2^-,SC]			
Gln [l]	[N,CO^-,SC]			[N,CO,SC]
Lys [m]	[N,CO^-,SC]			[N,CO,SC]
Arg [n]	[N,CO^-,SC]			[N,CO,SC],
				[N,CO^-]
His [o]	[N,CO^-,SC]		[N,CO^-,SC]	[N,CO,SC]

[a] Isomers are given in order of approximate relative population. SC = side-chain heteroatom or aromatic ring. [b] Ref. [216]. [c] Ref. [205]. [d] Ref. [213]. [e] Ref. [212]. [f] Ref. [218]. [g] Ref. [219]. [h] Ref. [200]. [i] Ref. [214]. L = acetonitrile or Asp. [j] Ref. [94]. [k] Ref. [93]. [l] Ref. [92]. [m] Ref. [95]. [n] Ref. [215]. [o] Ref. [211].

Figure Captions

Figure 1. Cross sections for collision-induced dissociation of Cs^+(Ser) with xenon as a function of kinetic energy in the center-of-mass frame (lower *x*-axis) and the laboratory frame (upper *x*-axis). The solid line shows the best fit to the data using the model discussed in the text convoluted over the neutral and ion kinetic and internal energy distributions. The dashed line shows the model cross section in the absence of experimental kinetic energy broadening for reactant ions with an internal energy of 0 K. Data and analysis taken from ref. [25].

Figure 2. Comparison of the experimental IRMPD action spectrum for Cs^+(Ser) with IR spectra for three low-lying conformations. Redrawn from ref. [64].

Figure 3. Types of metal-glycine coordination illustrated for Cs^+(Gly). Yellow dashed lines indicate metal coordination and light blue dotted lines indicate hydrogen bonds.

Figure 4. A potential energy surface calculated at the B3LYP/6-311+G(d,p) level for interconversion between K^+Ala[CO] and K^+Ala[CO,OH] as a function of KOC angle (part a) and between K^+Ala[CO,OH] and K^+Ala[CO_2^-] as a function of NH bond distance (part b).

Figure 5. Experimental 0 K bond dissociation energies (in kJ/mol) for M^+(Gly) (blue diamonds), M^+(Pro) (red circles), and M^+(Gln) (light green triangles) for $M^+ = Li^+$, Na^+, K^+, Rb^+, and Cs^+ are plotted versus the inverse metal cation radius (in $Å^{-1}$). The lines are linear regression fits to the data constrained to pass through the origin.

Figure 6. Types of metal-amino acid coordination illustrated by Cs^+(Ser) and Cs^+(Asp) (lower right). Yellow dashed lines indicate metal coordination and light blue dotted lines indicate hydrogen bonds.

Figure 7. IRMPD spectrum from ref. [155] compared to B3LYP/def2-TZVPPD calculated absorption spectra for conformers of Cs^+(Lys) with relative 298 K Gibbs energies (in kJ/mol)

calculated at the B3LYP/def2, M06/def2, and MP2/def2 levels.[150] Data taken from ref. [149] and calculated spectra from ref. [150].

Figure 8. Experimental 0 K bond dissociation energies (in kJ/mol) for Na^+(Xxx) (triangles), K^+(Xxx) (circles), and Cs^+(Xxx) (inverted triangles) versus the calculated polarizability (in $Å^3$) of the amino acid. The blue lines show linear regression analyses of the data in blue. Red and green lines are parallel to the regressions.

Figure 9. Experimental 0 K BDEs of M^+(L) versus the theoretical molecular polarizability of L = G, GG, GGG, GGGG and $M^+ = Na^+$ and K^+ taken from TCID (ref. [27], solid symbols) and kinetic method (ref. [175], open symbols) results. Full lines are regression fits to the TCID data. Dashed lines are the regression analyses from Figure 8.

Figure 10. Structures experimentally located for Zn^{2+} complexes with deprotonated aspartic acid. Part a shows the structure of $Zn(Asp\text{-}H)^+$ with an acetonitrile (ACN) ligand attached. Part b shows the structure found for $Zn(Asp\text{-}H)^+$, which has rearranged by eliminating ammonia. Yellow dashed lines indicate metal coordination and light blue dotted lines indicate hydrogen bonds.

Figure 11. Lowest energy structures of Zn complexes with histidine. Yellow dashed lines indicate metal coordination and light blue dotted lines indicate hydrogen bonds.

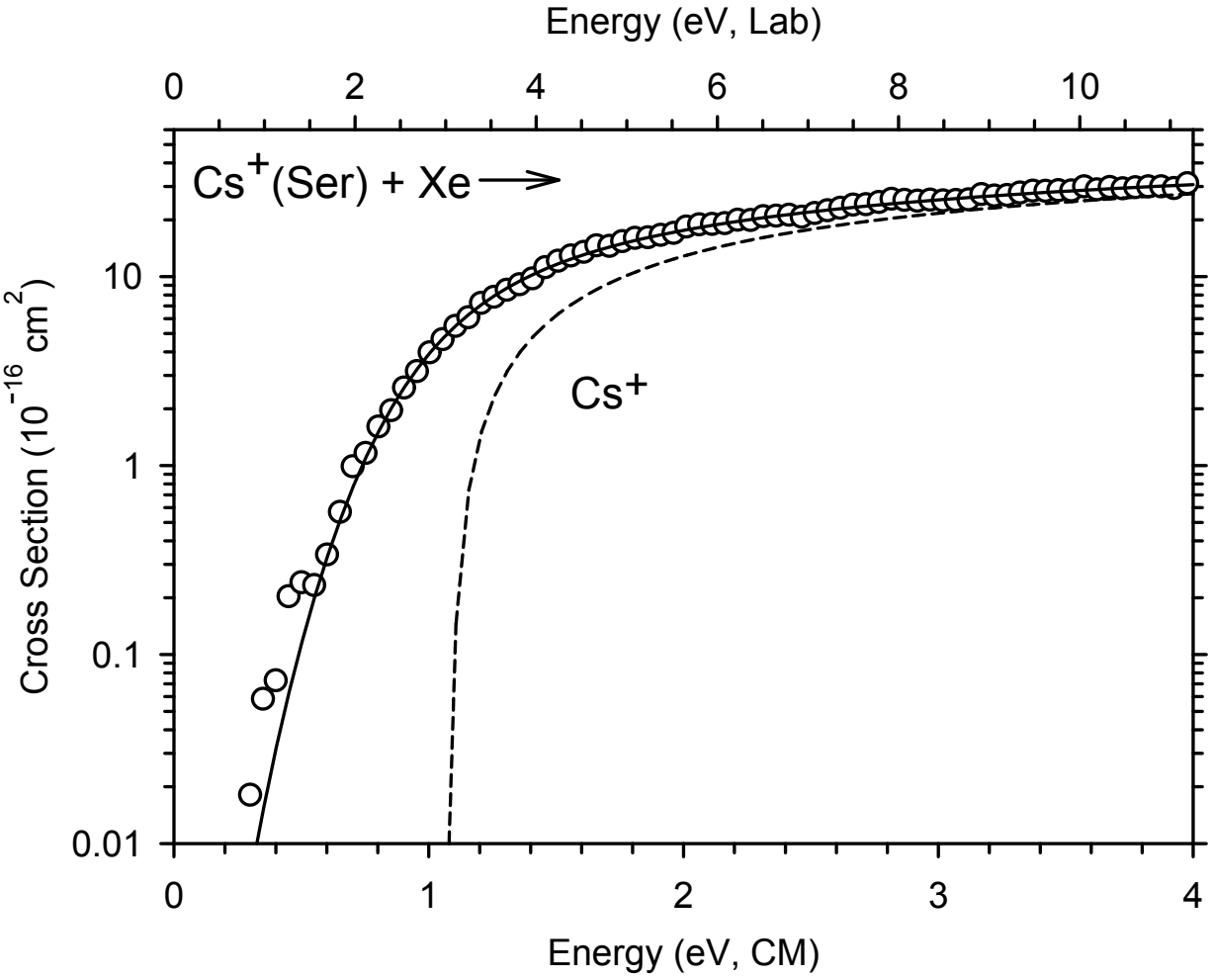
Energy (eV, Lab)
0
2
4
6
8
10
Cs+(Ser) + Xe
Cs+
Cross Section (10-16 cm2)
10
1
0.1
0.01
0
1
2
3
4
Energy (eV, CM)

Figure 1

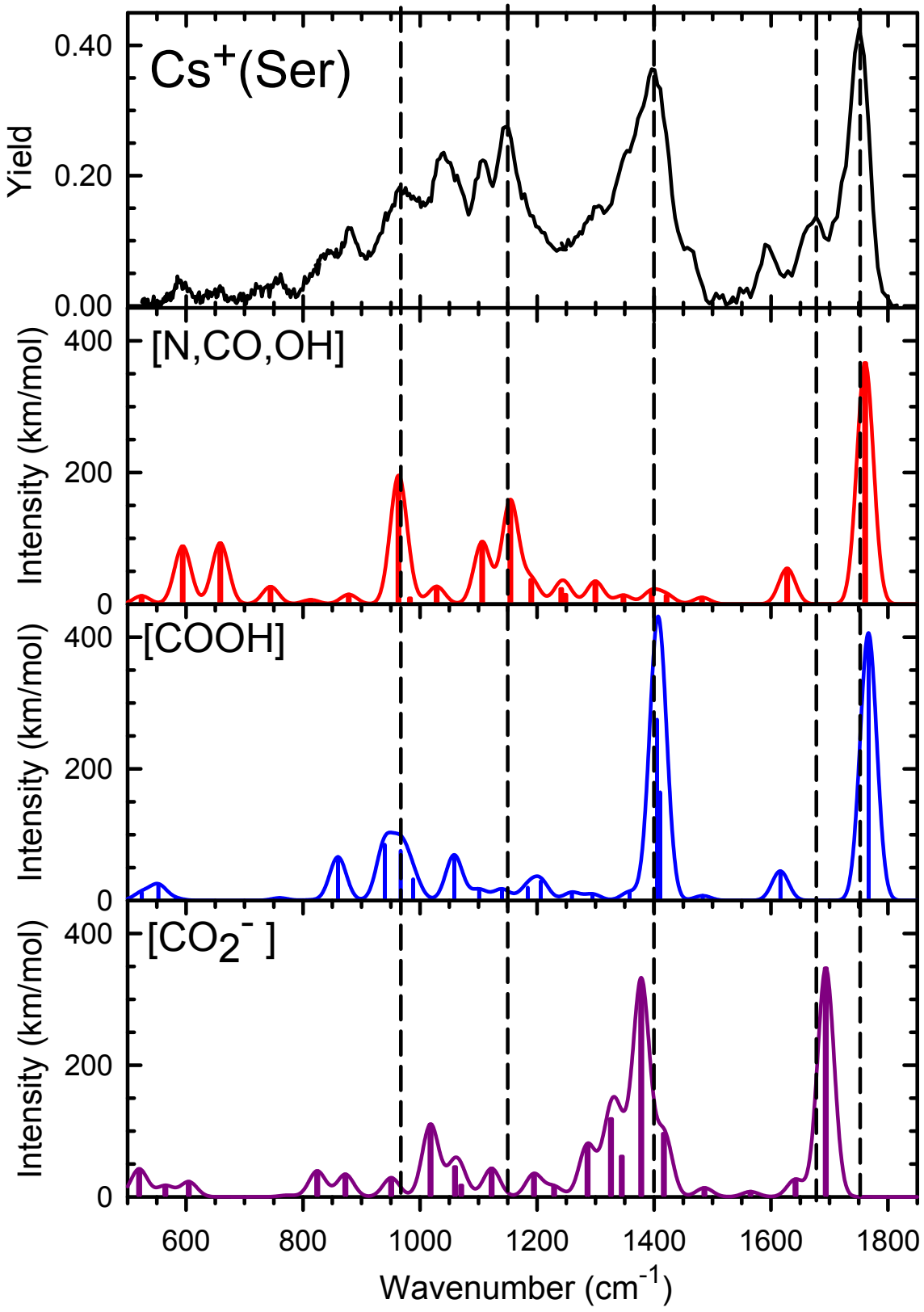
Cs+(Ser)
Yield
0.40
0.20
0.00
[N,CO,OH]
[COOH]
[CO2-]
Intensity (km/mol)
400
200
0
600
800
1000
1200
1400
1600
1800
Wavenumber (cm-1)

Figure 2

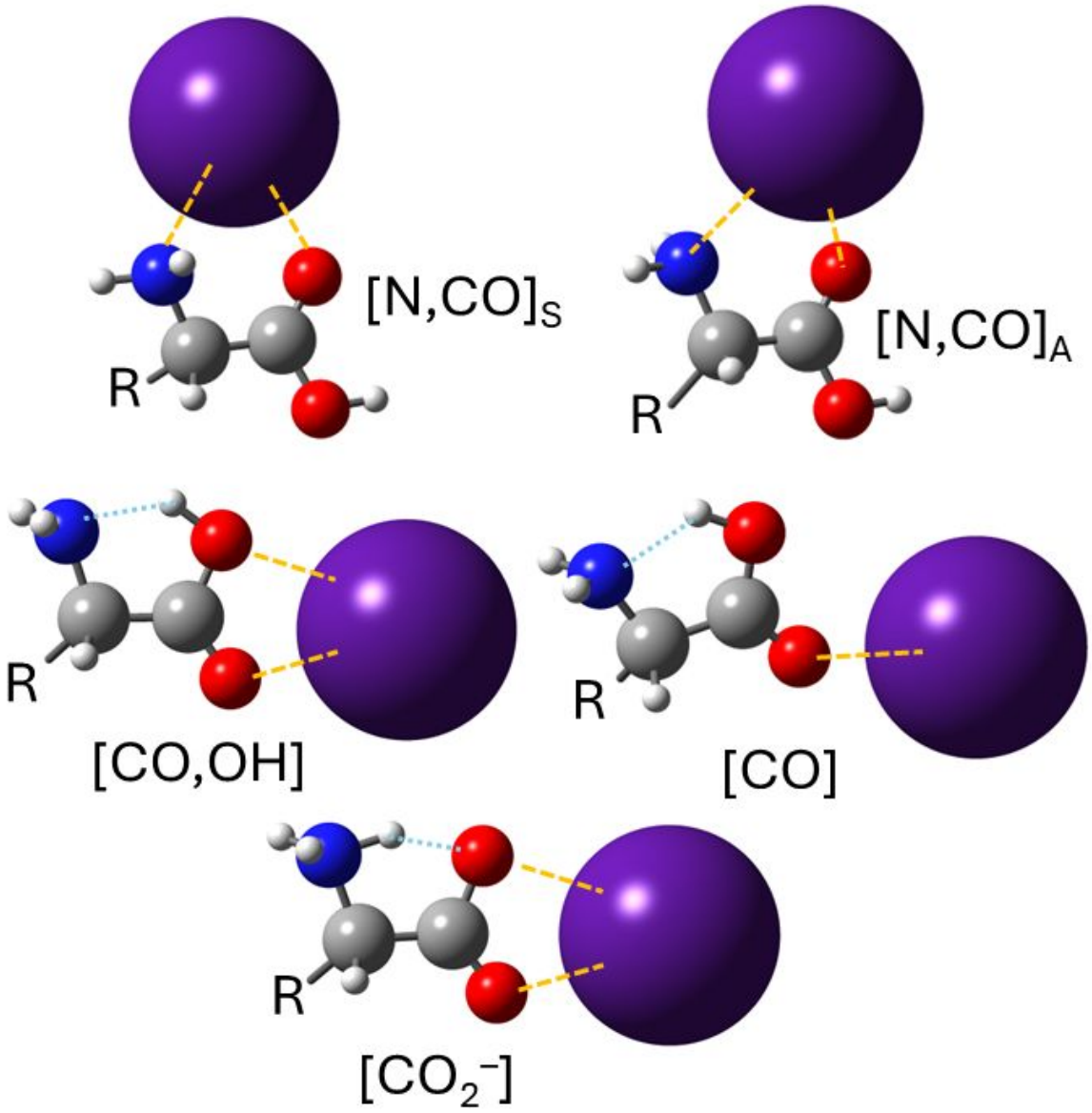

Figure 3

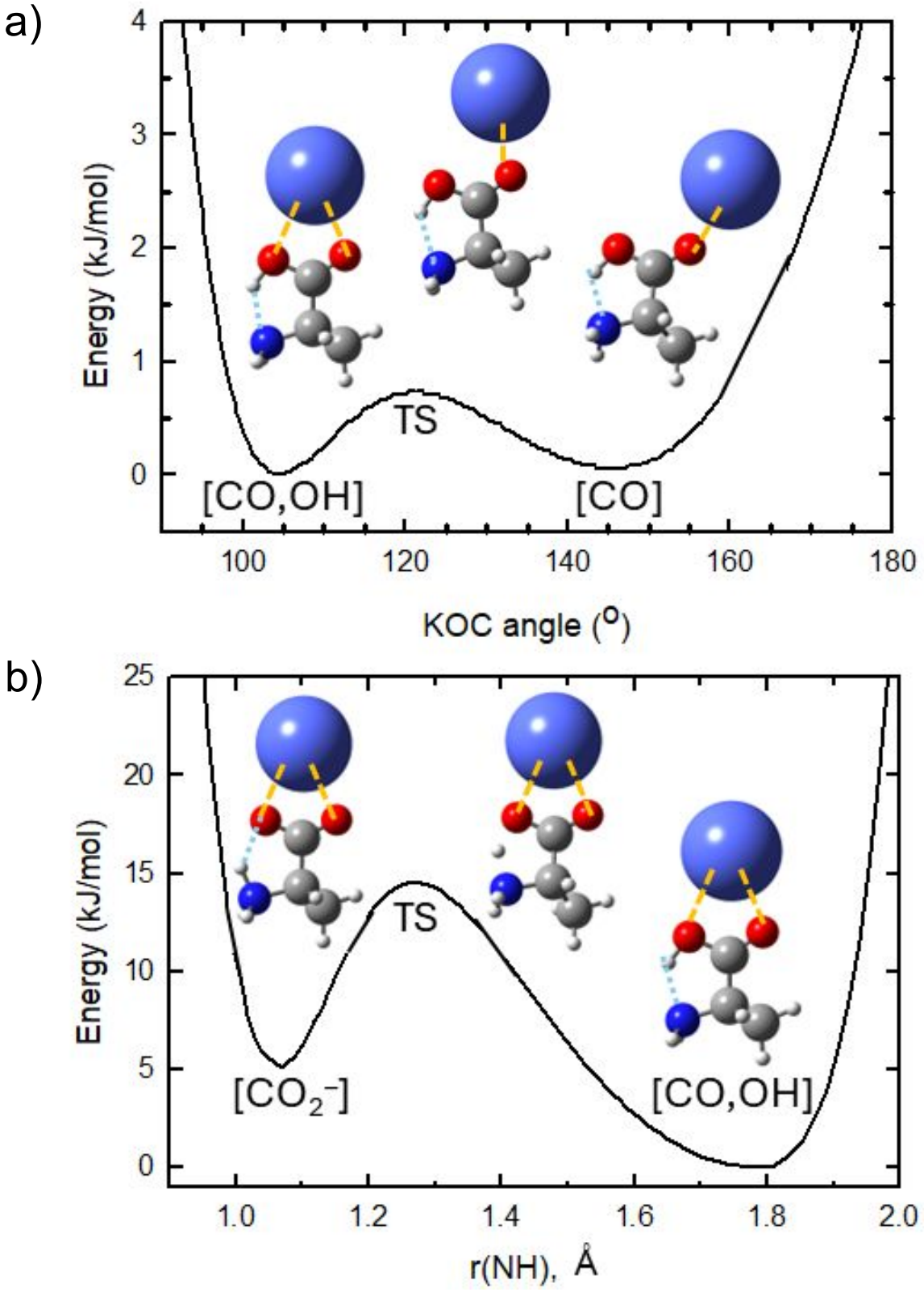
a)
Energy (kJ/mol)
KOC angle (°)
TS
[CO,OH]
[CO]
b)
Energy (kJ/mol)
r(NH), Å
TS
[CO2−]
[CO,OH]

Figure 4

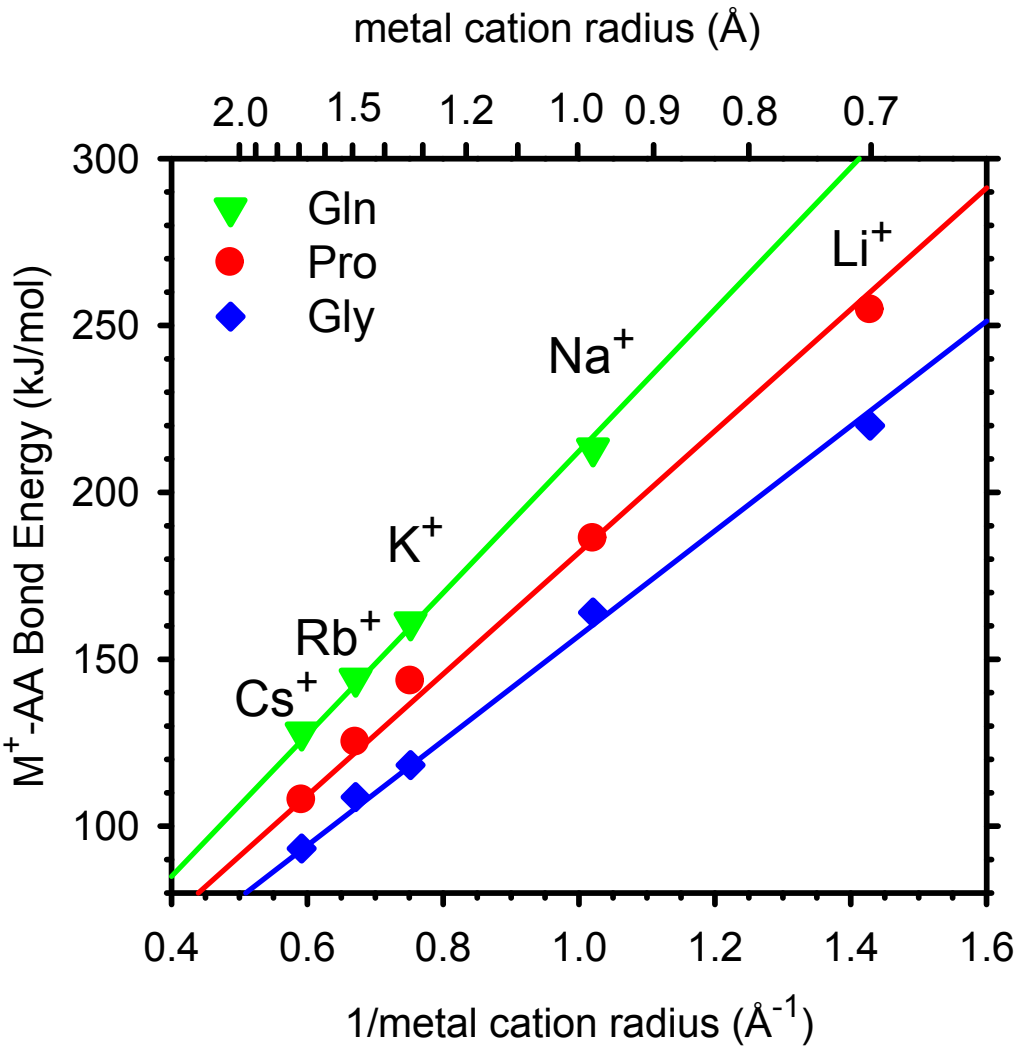
metal cation radius (Å)
2.0
1.5
1.2
1.0
0.9
0.8
0.7
300
250
200
150
100
M+-AA Bond Energy (kJ/mol)
Gln
Pro
Gly
Li+
Na+
K+
Rb+
Cs+
0.4
0.6
0.8
1.0
1.2
1.4
1.6
1/metal cation radius (Å-1)

Figure 5

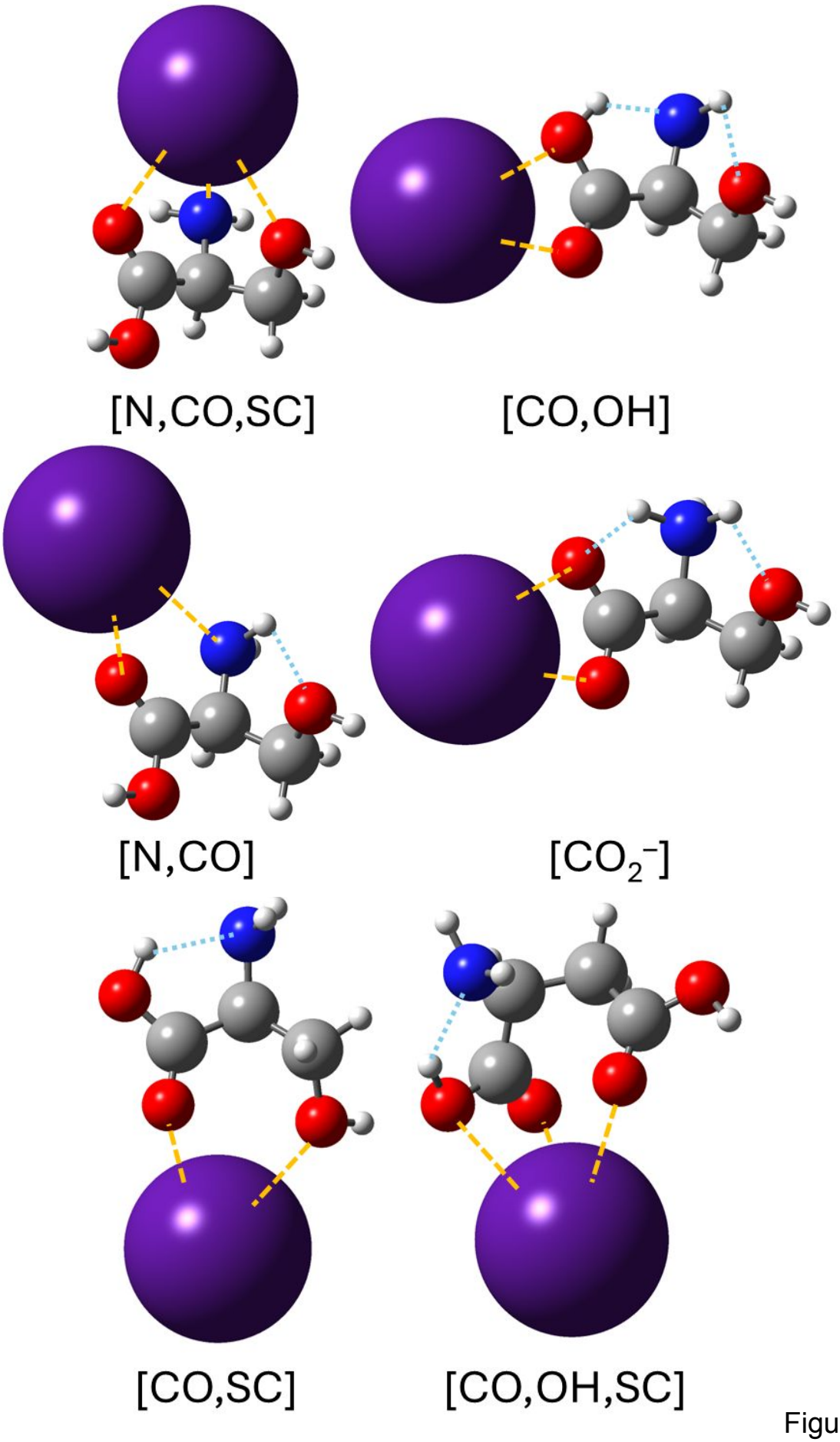

Figure 6

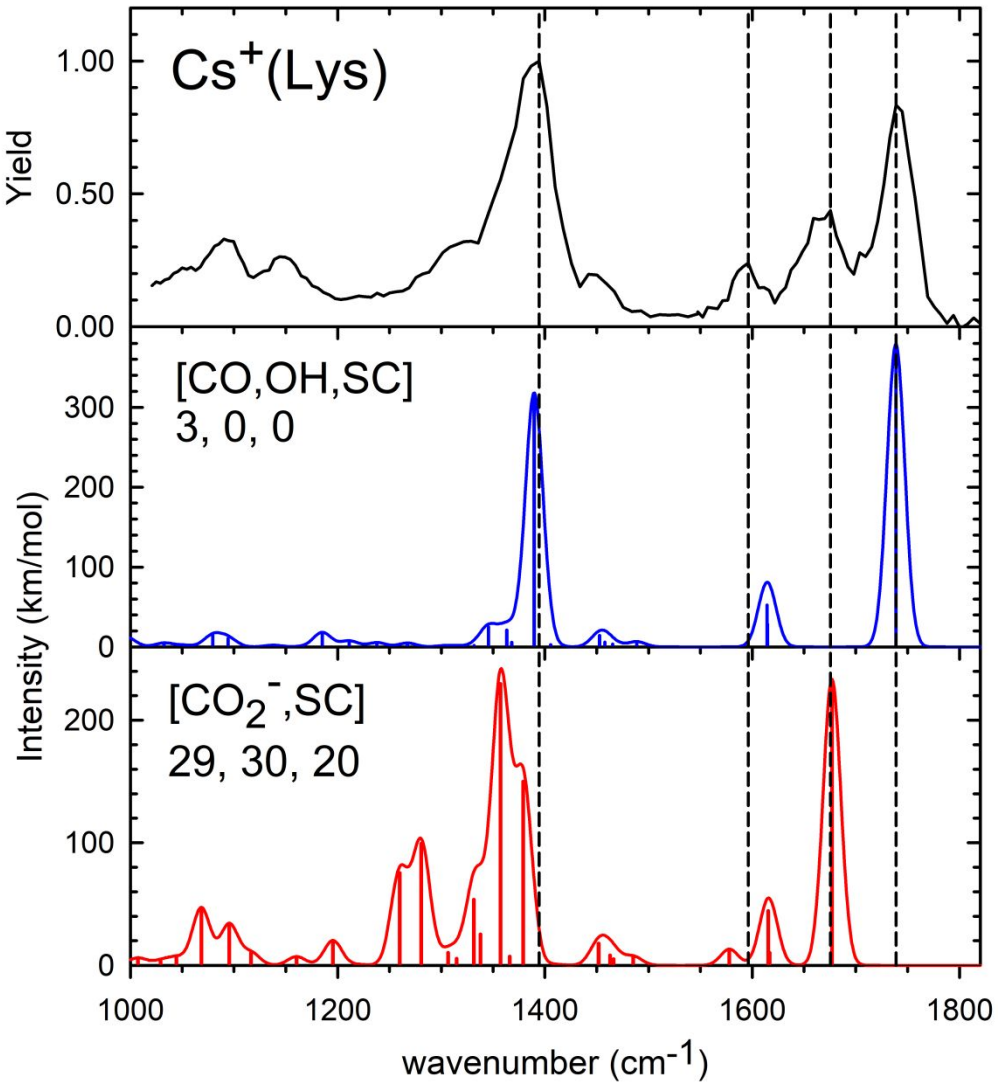
Cs+(Lys)
Yield
1.00
0.50
0.00
[CO,OH,SC]
3, 0, 0
300
200
100
0
Intensity (km/mol)
[CO2-,SC]
29, 30, 20
200
100
0
1000
1200
1400
1600
1800
wavenumber (cm-1)

Figure 7

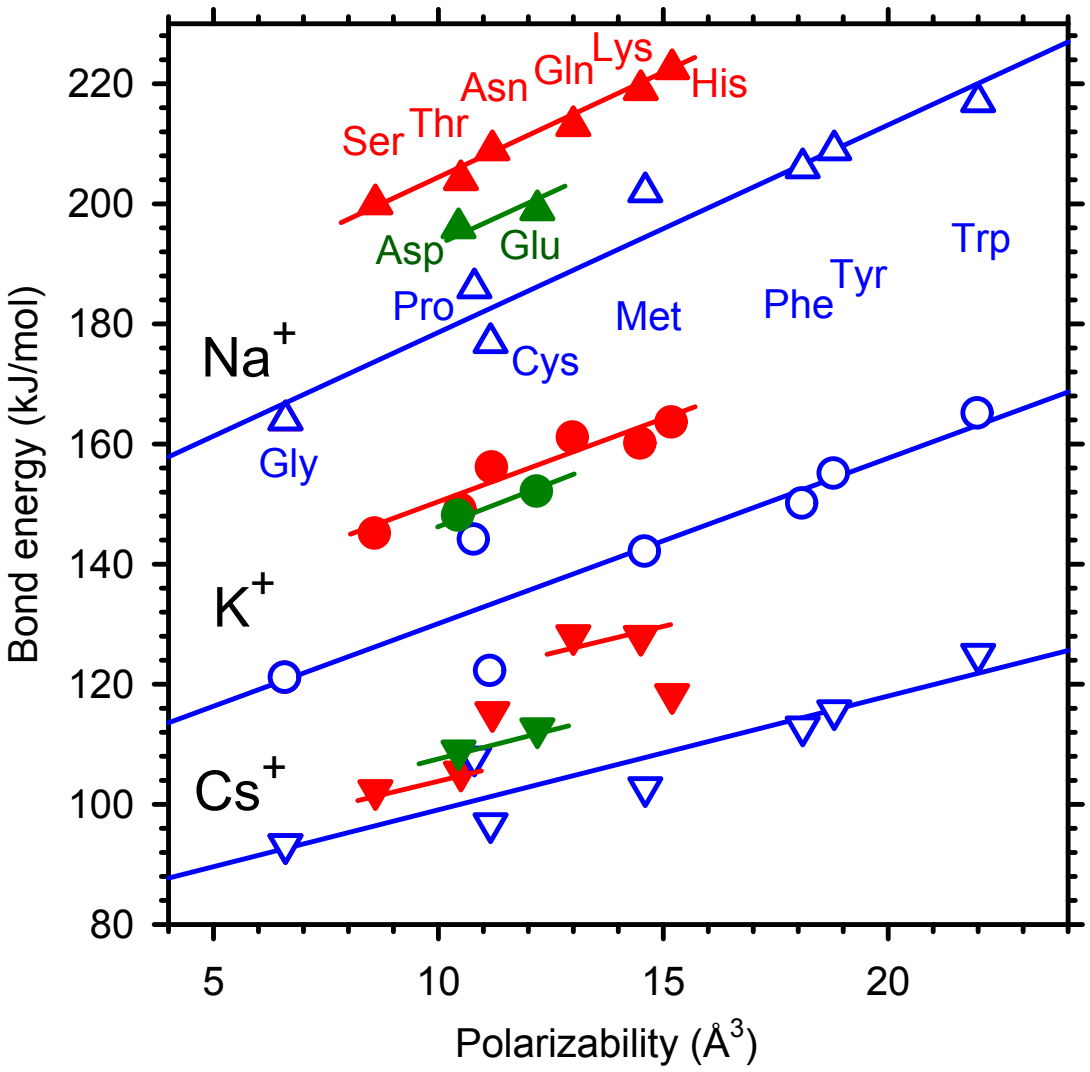
Bond energy (kJ/mol)
Polarizability (Å^3)
220
200
180
160
140
120
100
80
5
10
15
20
Na$^+$
K$^+$
Cs$^+$
Ser
Thr
Asn
Gln
Lys
His
Asp
Glu
Pro
Cys
Met
Phe
Tyr
Trp
Gly

Figure 8

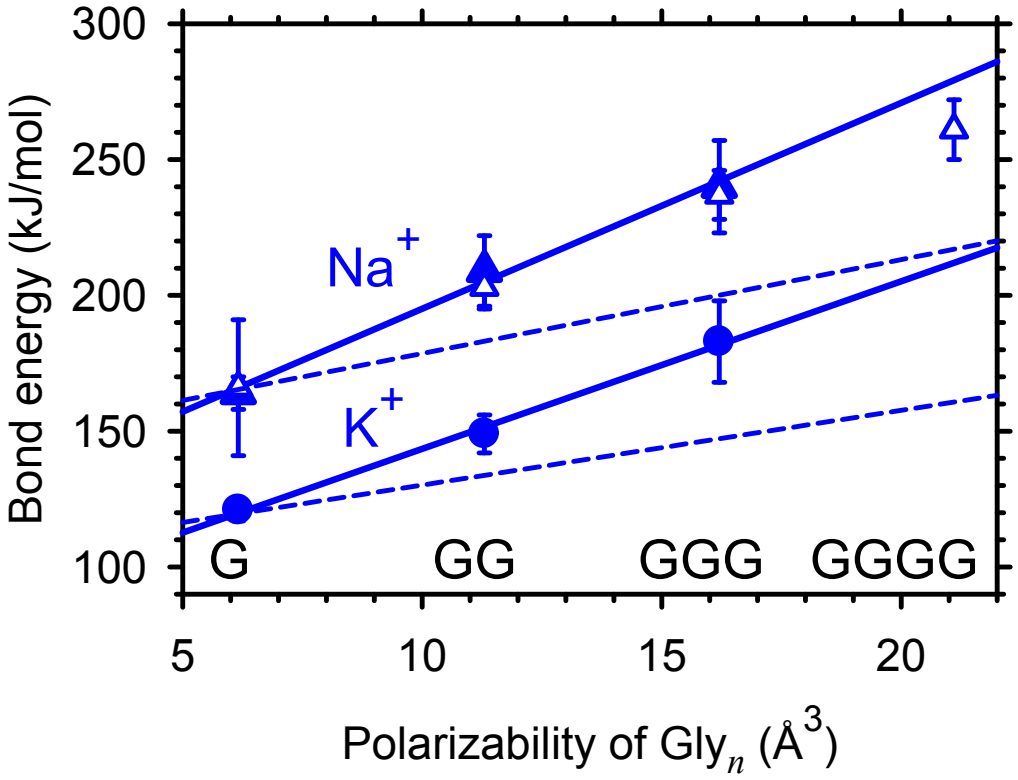
300
250
200
150
100
Bond energy (kJ/mol)
Na+
K+
G
GG
GGG
GGGG
5
10
15
20
Polarizability of Gly$_n$ (Å^3)

Figure 9

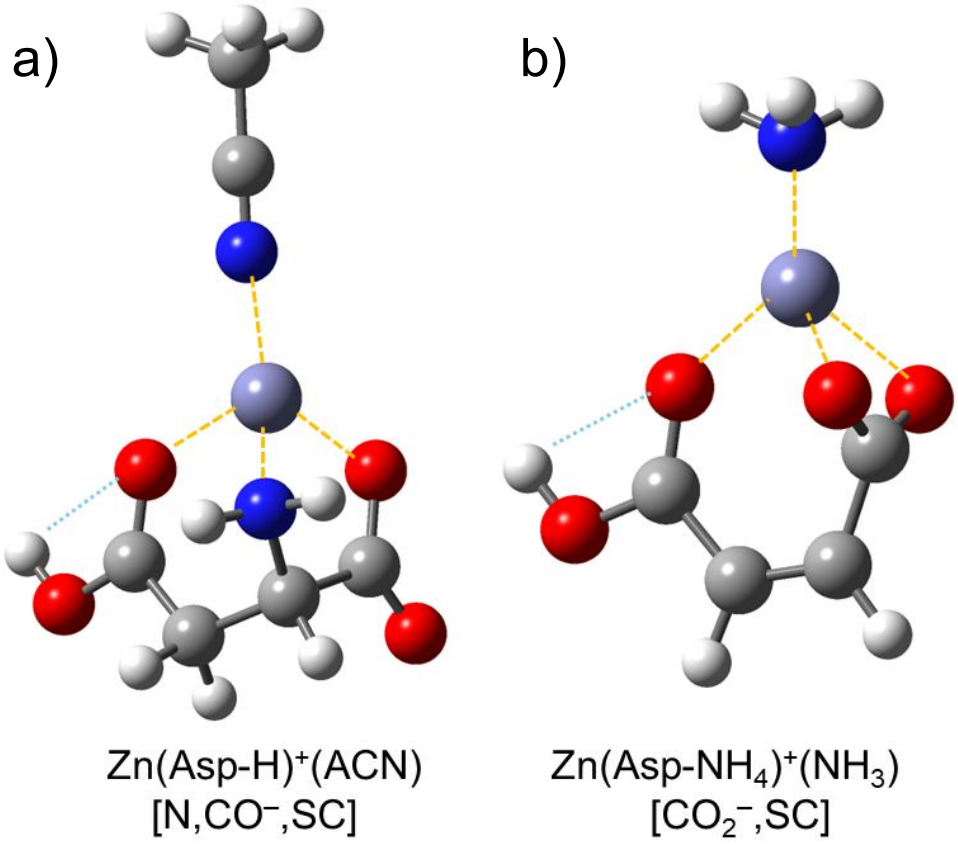

Figure 10

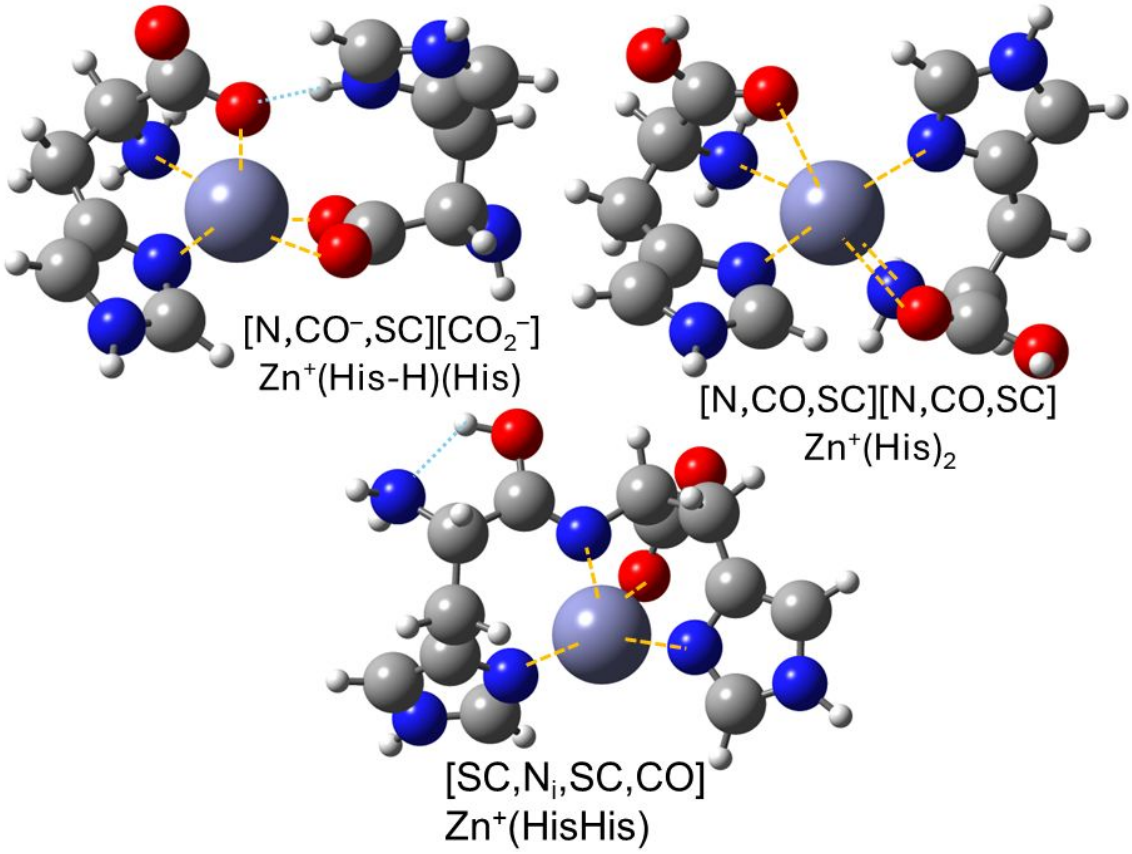

Figure 11

- No primary research results, software or code have been included and no new data were generated or analysed as part of this review.